

U-learning for Prediction Inference via Combinatory Multi-Subsampling: With Applications to LASSO and Neural Networks

Zhe Fei

*Department of Statistics
University of California, Riverside
Riverside, CA 92521, USA*

ZHE.FEI@UCR.EDU

Yi Li

*Department of Biostatistics
University of Michigan
Ann Arbor, MI, 48109, USA*

YILI@UMICH.EDU

Editor: My editor

Abstract

Epigenetic aging clocks play a pivotal role in estimating an individual's biological age through the examination of DNA methylation patterns at numerous CpG (Cytosine-phosphate-Guanine) sites within their genome. However, making valid inferences on predicted epigenetic ages, or more broadly, on predictions derived from high-dimensional inputs, presents challenges. We introduce a novel U-learning approach via combinatorial multi-subsampling for making ensemble predictions and constructing confidence intervals for predictions of continuous outcomes when traditional asymptotic methods are not applicable. More specifically, our approach conceptualizes the ensemble estimators within the framework of generalized U-statistics and invokes the Hájek projection for deriving the variances of predictions and constructing confidence intervals with valid conditional coverage probabilities. We apply our approach to two commonly used predictive algorithms, Lasso and deep neural networks (DNNs), and illustrate the validity of inferences with extensive numerical studies. We have applied these methods to predict the DNA methylation age (DNAmAge) of patients with various health conditions, aiming to accurately characterize the aging process and potentially guide anti-aging interventions.

Keywords: Ensemble Learning, DNN, Incomplete Generalized U-Statistics, Prediction Interval, Subsampling

1 Introduction

Epigenetic aging clocks, composed of CpG sites and their DNA methylation levels, are designed to predict 'methylation ages' of subjects, commonly known as DNA methylation ages (DNAmAge). While it strongly correlates with chronological age, DNAmAge provides a more nuanced reflection of the aging process, telling if a person ages slower or faster than the expectation. Consequently, there is a pressing need to obtain accurate uncertainty measures, which are essential for evaluating biological aging rates. More broadly, the challenge lies in making predictions and inferences with complex, often less-interpretable machine learning models, a common issue in modern learning tasks.

Much progress has been achieved in high-dimensional inference, particularly in the realm of estimating parameters whose dimensionality surpasses the sample size. The methods encompass de-biased approaches (Zhang and Zhang, 2014; Javanmard and Montanari, 2014), post-selection exact inference (Lee et al., 2016; Belloni et al., 2016), and many more (Ning and Liu, 2017; Fei et al., 2019; Zhu and Bradic, 2018; Fei and Li, 2021). Moreover, extensions to non-linear models have also been explored (Van de Geer et al., 2014; Kong et al., 2021; Fei et al., 2023). However, none of these works address the uncertainty associated with individual predictions, as they aim to make inferences about model parameters or the effects of predictors, which fundamentally differs from inferring subject-specific predictions.

A notable area that connects high-dimensional inference with prediction inference is the task of inferring treatment effects amidst high-dimensional confounders (Belloni et al., 2014a,b; Avagyan and Vansteelandt, 2022). This is because treatment effects are often estimated as the differences in outcomes under different treatment assignments. Important developments include the methods based on regression trees and random forests (Wager and Athey, 2018), debiasing (Athey et al., 2018), and estimating dynamic treatment effects within marginal structural models (Bradic et al., 2021).

Recent research in prediction inference yields several techniques, including a residual-based bootstrap method with adjustment to guarantee conditional validity and marginal coverage (Zhang and Politis, 2023); the distribution-free conformal inference (Lei et al., 2018; Angelopoulos and Bates, 2021; Kato et al., 2023); extension of the Jackknife inference (Kim et al., 2020; Barber et al., 2021); applications of sub-sampling and U-statistics to regressions and neural networks (Schupbach et al., 2020; Wang and Wei, 2022); and lower upper bound estimation method for neural networks-based prediction intervals (Khosravi et al., 2010). Extending beyond continuous outcomes, Guo et al. (2021) focuses on inference for the case probability in high-dimensional logistic regressions, using an extension of the debiased/projection estimator. Limitations are present with these methods. For example, the bootstrap-based approach detailed in Zhang and Politis (2023) is primarily applicable to linear regression models, which may not cover the full spectrum of prediction scenarios; Schupbach et al. (2020), Wang and Wei (2022) and Khosravi et al. (2010) provide limited theoretical justifications of their methods. Mentch and Hooker (2016) derives theoretical results and properties of U-statistics for quantifying prediction uncertainty in random forests. However, it is unclear whether these theories can be directly applied to Lasso or deep learning algorithms. Various conformal prediction methods often impose assumptions like exchangeability, strongly mixing errors, or covariate shift (Papadopoulos et al., 2007; Tibshirani et al., 2019; Romano et al., 2020; Chernozhukov et al., 2021), and tend to be conservative with wide intervals. Moreover, since conformal prediction derives the conformity score based on the *observed outcomes*, it fails to distinguish measurement errors within the observations. This would result in less efficiency compared to methods that directly model the distribution of *true outcomes*.

To tackle these challenges, we aim to predict future outcomes and accurately assess the associated uncertainty. This is particularly pertinent with less structured algorithms where established inference techniques are not readily available. In the motivating epigenetic project, we use penalized regressions and deep neural networks to predict subject-specific methylation ages, and it is crucial to determine whether these predictions are statistically significantly different from the chronological ages. To improve prediction accuracy with high

dimensional features, we propose an ensemble approach that originates from U-statistics, and resort to the Hájek projection properties for variance estimation and inference. The ensemble prediction improves the efficiency and leads to tractable asymptotics and valid inferences. Intuitively, the proposed approach extends random forests, which ensemble decision trees, to the ensembles of regressions and neural networks.

Our method offers several advantages over existing approaches: i) our ensemble learners are asymptotically normal, a result proven through a careful derivation from generalized U-statistic properties (Mentch and Hooker, 2016); ii) our variance estimator is model-free, requiring minimal assumptions, owing to the Hájek projection properties (Hoeffding, 1992; Hájek, 1968; Wager and Athey, 2018); iii) our confidence intervals are tailored to individual future subjects, providing *conditional* coverage, in contrast to *marginal* coverage at the population level, thereby enhancing applicability. A key contribution is the formulation of ensemble predictions, based on Lasso or neural networks, as incomplete U-statistics, leading to the tractable asymptotics (Janson, 1984; Frees, 1989; Lee, 2019).

In Section 2, we introduce the models and proposed methods. This is followed by a discussion of theoretical properties in Section 3 and the presentation of numerical examples in Section 4. Section 5 delves into detailed analyses of the DNA methylation data, illustrating the development of new epigenetic aging clocks using our proposed methods. Section 6 concludes the paper with remarks and outlines of future directions.

2 U-learning for Prediction Inference

Assume the observed data of size n , $\mathcal{T}_n = \{Z_i = (y_i, \mathbf{x}_i) : i = 1, \dots, n\}$, are independently and identically distributed (i.i.d.) copies of (y, \mathbf{x}) , with $y \in \mathbb{R}^1$ and $\mathbf{x} \in \mathbb{R}^{1 \times p}$ satisfying

$$y = f_0(\mathbf{x}) + \varepsilon, \tag{1}$$

where $f_0 : \mathbb{R}^p \rightarrow \mathbb{R}$ is a function quantifying the dependence of the expectation of y on \mathbf{x} , and ε is a mean zero error term that is independent of \mathbf{x} . We assume that \mathbf{x} follows an unspecified distribution of \mathcal{X} . We define a compatible prediction problem: given a fixed \mathbf{x}_* in the support of \mathcal{X} , suppose the associated outcome y_* follows (1) but is unobserved. The goal of the paper centers on predicting $E(y_*|\mathbf{x}_*) = f_0(\mathbf{x}_*)$ based on \mathcal{T}_n . If we obtain a ‘good’ estimate of $f_0(\cdot)$, denoted by $\hat{f}(\cdot)$, from Lasso or a deep neural network (DNN), we would predict $f_0(\mathbf{x}_*)$ via $\hat{f}(\mathbf{x}_*)$. To quantify the prediction uncertainty, we will derive a confidence interval $(\hat{L}(\mathbf{x}_*), \hat{U}(\mathbf{x}_*))$ that covers $f_0(\mathbf{x}_*)$ with a target probability of $0 < 1 - \alpha < 1$. That is,

$$\Pr \left[f_0(\mathbf{x}_*) \in \left(\hat{L}(\mathbf{x}_*), \hat{U}(\mathbf{x}_*) \right) \right] \rightarrow 1 - \alpha, \quad \text{as } n \rightarrow \infty.$$

Intuitively, if $\hat{y}_* = \hat{f}(\mathbf{x}_*)$ is a consistent estimate of $f_0(\mathbf{x}_*)$, and is asymptotically normal, an approximate confidence interval based on a normal distribution can be obtained by estimating the *prediction error variance*, $\sigma_*^2 \equiv \text{Var} \left(\hat{f}(\mathbf{x}_*) \right)$. In machine learning, however, making predictions based on a single dataset typically leads to significant variations, and its large sample properties are often intractable (Andreassen and Dyer, 2020; Zavatone-Veth et al., 2021).

As a general approach, we propose below a combinatory multi-subsampling (CMS) scheme that provides an ensemble prediction with tractable asymptotics and model-free

variance estimates. This scheme can be applied to many commonly used machine learning algorithms, including Lasso and neural networks. For the index set $\mathcal{I} = \{1, \dots, n\}$ of the training data \mathcal{T}_n , there are $B^* = \binom{n}{r}$ combinations of unique subsets of size $r (< n)$. We enumerate these unique subsets from 1 to B^* (e.g., in the lexical order), and denote each one as $\mathcal{I}^{\dot{b}} = \{i_1, \dots, i_r\}$ with $i_1 < \dots < i_r$ and $\dot{b} = 1, \dots, B^*$.

1. For each $\dot{b} = 1, 2, \dots, B^*$, subsample r observations (without replacement) with the index set $\mathcal{I}^{\dot{b}} = \{i_1, \dots, i_r\}$ from the original samples \mathcal{T}_n . Denote by $\mathcal{I}_V^{\dot{b}} = \mathcal{I} \setminus \mathcal{I}^{\dot{b}}$.
2. Train the model with observations indexed by $\mathcal{I}^{\dot{b}}$, and use observations indexed by $\mathcal{I}_V^{\dot{b}}$ for model selection/hyperparameter tuning. Denote the trained model by $\tilde{f}^{\dot{b}}$.
3. Apply $\tilde{f}^{\dot{b}}$ to a testing point \mathbf{x}_* and denote the prediction as $\tilde{f}^{\dot{b}}(\mathbf{x}_*)$. Compute the ensemble prediction as

$$\hat{f}^{B^*}(\mathbf{x}_*) = \frac{1}{B^*} \sum_{\dot{b}=1}^{B^*} \tilde{f}^{\dot{b}}(\mathbf{x}_*).$$

4. Compute the variance estimator by infinitesimal jackknife (introduced in the next subsection) as $\hat{\sigma}_*^2$ and derive the confidence interval for prediction (CIP) as

$$\left(\hat{f}^{B^*}(\mathbf{x}_*) - c_\alpha \hat{\sigma}_*, \hat{f}^{B^*}(\mathbf{x}_*) + c_\alpha \hat{\sigma}_* \right),$$

where c_α controls the $(1 - \alpha)$ confidence level with a given $0 < \alpha < 1$.

We will use generalized U-statistic theories to derive the asymptotic properties of $\hat{f}^{B^*}(\mathbf{x}_*)$ and to draw inference, thus our procedure is termed *U-learning* for prediction and inference. In practice, we allow r to increase along with n (denoted as r_n). As computing all B^* models is not feasible even with moderate r and n , we propose a stochastic approximation with a suitable B for implementing the U-learning procedure.

2.1 Application to prediction with the LASSO

Consider a linear version of Model (1), i.e.,

$$y_i = f_0(\mathbf{x}_i) + \varepsilon_i = \beta_0^0 + \mathbf{x}_i \boldsymbol{\beta}^0 + \varepsilon_i, \quad i = 1, \dots, n, \quad (2)$$

where $\mathbf{x}_i = (x_{i1}, \dots, x_{ip})$, and $f_0(\mathbf{x}) = \beta_0^0 + \mathbf{x} \boldsymbol{\beta}^0$. Denote the response vector and design matrix of \mathcal{T}_n by $\mathbf{Y} = (y_1, \dots, y_n)^T$ and $\mathbf{X} = (\mathbf{x}_1^T, \dots, \mathbf{x}_n^T)^T$, respectively. For $\dot{b} = 1, 2, \dots, B^*$, denote by $\mathcal{T}^{\dot{b}} = (\mathbf{Y}_{\mathcal{I}^{\dot{b}}}, \mathbf{X}_{\mathcal{I}^{\dot{b}}})$, where $\mathbf{Y}_{\mathcal{I}^{\dot{b}}}$ and $\mathbf{X}_{\mathcal{I}^{\dot{b}}}$ are, respectively, a subvector of \mathbf{Y} and a submatrix of \mathbf{X} with rows indexed by $\mathcal{I}^{\dot{b}}$. In high dimensional settings, where classic linear regressions are not applicable, we apply Lasso to fit model (2) and obtain the estimates of β_0^0 and $\boldsymbol{\beta}^0$:

$$\left(\tilde{\beta}_0^{\dot{b}}, \tilde{\boldsymbol{\beta}}^{\dot{b}} \right) = \underset{(\beta_0, \boldsymbol{\beta}): \|\boldsymbol{\beta}\|_1 < K}{\operatorname{argmin}} \|\mathbf{Y}_{\mathcal{I}^{\dot{b}}} - \beta_0 \mathbf{1}_r - \mathbf{X}_{\mathcal{I}^{\dot{b}}} \boldsymbol{\beta}\|_2^2, \quad (3)$$

where $\mathbf{1}_r$ is an r -dimensional vector of 1's, and K is a pre-defined positive constant. This formulation is equivalent to the unconstrained optimization problem of ‘‘Loss + Penalty’’.

Then for any fixed \mathbf{x}_* in the support of \mathcal{X} , the Lasso prediction based on the subsample $\mathcal{T}^{\dot{b}}$ is

$$\hat{y}_*^{\dot{b}} = \tilde{f}(\mathbf{x}_*; \mathcal{T}^{\dot{b}}) = \tilde{\beta}_0^{\dot{b}} + \mathbf{x}_* \tilde{\beta}^{\dot{b}}. \quad (4)$$

In general, the Lasso prediction $\hat{y}_*^{\dot{b}}$ based on a single dataset incurs considerable variation, and its distribution is not tractable (Fu and Knight, 2000), even when the sample size is large, thus making inference rather challenging. A key observation, however, is that with a fixed K , $\hat{y}_*^{\dot{b}}$ is permutation symmetric with respect to $\mathcal{I}^{\dot{b}}$. Hence, the ensemble prediction

$$\tilde{y}_*^\infty = \left(\sum_{\dot{b}=1}^{B^*} \hat{y}_*^{\dot{b}} \right) / \binom{n}{r} \quad (5)$$

is indeed a generalized U-statistic (Lee, 2019), which can be shown to be a consistent estimator of $f_0(\mathbf{x}_*)$ and is asymptotically normal. Moreover, its U-statistic structure leads to an estimate of its variance via the Hájek projection, facilitating construction of confidence intervals. The formulation of (5) is general; when $r = n - 1$ and thus $B^* = n$, (5) includes the Jackknife estimate as a special case.

Computing \tilde{y}_*^∞ requires fitting $\binom{n}{r}$ regression models, which is impractical even with moderate r and n . We propose a stochastic approximation of (5) with a sufficiently large B . That is, randomly draw B size- r subsamples from the original data \mathcal{T}_n . In term of probability, this can be described as independently generate b_1, \dots, b_B , where each b_j is chosen from 1 to $\binom{n}{r}$ with equal probability, i.e., $\Pr(b_j = \dot{b}) = 1/\binom{n}{r}$ for $\dot{b} \in \{1, \dots, \binom{n}{r}\}$, and the j -th size- r subsample is indexed by \mathcal{I}^{b_j} , $j = 1, \dots, B$. With this notion and as described in Algorithm 1, we propose the U-learning prediction

$$\hat{y}_*^B = \frac{1}{B} \sum_{j=1}^B (\tilde{\beta}_0^{b_j} + \mathbf{x}_* \tilde{\beta}^{b_j}) = \frac{1}{B} \sum_{j=1}^B \hat{y}_*^{b_j}, \quad (6)$$

where each $\tilde{\beta}_0^{b_j}$ and $\tilde{\beta}^{b_j}$ are the Lasso estimates from (3) based on the sub-sampled data \mathcal{T}^{b_j} . By the law of large numbers, (6) approximates (5) well as B increases. With a U-statistic framework, we term the prediction (6) *Lasso U-learning*.

As (6) is an ensemble prediction based on subsampling, we apply the infinitesimal jackknife method (Wager and Athey, 2018; Fei and Li, 2021) to obtain a variance estimator of $\hat{f}^B(\mathbf{x}_*)$ as

$$\hat{\sigma}_*^2 = \frac{n-1}{n} \left(\frac{n}{n-r} \right)^2 \sum_{i=1}^n \widehat{\text{Cov}}_{i,*}^2 \quad (7)$$

where the sampling covariance is

$$\widehat{\text{Cov}}_{i,*} = \frac{\sum_{j=1}^B (J_{b_j i} - J_{\cdot i})(\hat{y}_*^{b_j} - \hat{y}_*^B)}{B},$$

where $J_{b_j i} = I(i \in \mathcal{I}^{b_j})$ and $J_{\cdot i} = \frac{1}{B} \sum_{j=1}^B J_{b_j i}$.

Algorithm 1 Lasso U-learning prediction and inference

Require: Subsampling size r , and number of subsamples B **Input:** Training data \mathcal{T}_n , Lasso constraint K , and a fixed test point \mathbf{x}_* **Output:** Prediction \hat{y}_*^B and $100(1 - \alpha)\%$ confidence interval $(\hat{L}(\mathbf{x}_*), \hat{U}(\mathbf{x}_*))$

- 1: **for** $j = 1, 2, \dots, B$ **do**
 - 2: Random subsample data of size r without replacement. Denote by \mathcal{T}^{b_j} the resampled data (indexed by \mathcal{I}^{b_j}), and save the sampling vector $\mathbf{J}_{b_j} = (J_{b_j1}, \dots, J_{b_jn})$
 - 3: Fit Lasso on \mathcal{T}^{b_j} with the constraint constant K and output $\tilde{\beta}_0^{b_j}, \tilde{\beta}^{b_j}$
 - 4: Predict $\hat{y}_*^{b_j} = \tilde{\beta}_0^{b_j} + \mathbf{x}_* \tilde{\beta}^{b_j}$
 - 5: **end for**
 - 6: Compute \hat{y}_*^B by (6) and $\hat{\sigma}_*^2$ by (7)
 - 7: Compute a $100(1 - \alpha)\%$ confidence interval for $f_0(\mathbf{x}_*)$ as $(\hat{y}_*^B - z_{1-\alpha/2} \hat{\sigma}_*, \hat{y}_*^B + z_{1-\alpha/2} \hat{\sigma}_*)$
-

2.2 Application to prediction with deep neural networks

Deep neural networks have emerged as a powerful means for nonparametric regression. We use neural networks to fit a nonparametric version of Model (1), where $f_0(\cdot) : [0, 1]^p \rightarrow \mathbb{R}$ is an unknown truth satisfying certain smoothness conditions. The basic unit of a neural network is a neuron, which takes input values, processes them using weights and biases (intercepts), and produces an output value. Denote the input values as a row vector \mathbf{x} , the weights as column vector \mathbf{w} and the bias term as a . The output of a neuron is calculated by applying an activation function, denoted by $\sigma : \mathbb{R} \rightarrow \mathbb{R}$, to a weighted sum of its inputs plus an intercept (bias): $v = \sigma(\mathbf{x}\mathbf{w} + a)$. For the purpose of the theoretical derivations, we restrict to the ReLU activation function in this paper, i.e., $\sigma(x) = \max(x, 0)$.

A multilayer neural network or a deep neural network (DNN) consists of multiple layers of interconnected neurons with a specific network architecture (L, \mathbf{p}) , where L is the number of hidden layers, and $\mathbf{p} = (p_0, p_1, \dots, p_{L+1}) \in \mathbb{N}^{L+2}$ the width vector (Schmidt-Hieber, 2020). Then a DNN can be expressed as

$$f : \mathbb{R}^{p_0} \rightarrow \mathbb{R}^{p_{L+1}},$$

$$\mathbf{x} \mapsto f(\mathbf{x}) = \mathbf{W}_L \sigma_L(\mathbf{W}_{L-1} \sigma_{L-1}(\dots \mathbf{W}_1 \sigma_1(\mathbf{W}_0 \mathbf{x}^T + \mathbf{a}_0) + \mathbf{a}_1) \dots + \mathbf{a}_{L-1}) + \mathbf{a}_L, \quad (8)$$

where \mathbf{W}_ℓ 's are $p_{\ell+1} \times p_\ell$ weight matrices and \mathbf{a}_ℓ 's are the intercept vector, and $\sigma_\ell(\cdot)$'s are activation functions operating on vectors element-wise. In our setting, $p_0 = p$ and $p_{L+1} = 1$. We denote $\mathcal{F}(L, \mathbf{p})$ as the class of functions defined in (8) with L hidden layers and the width vector \mathbf{p} . There is a natural extension of Algorithm 1 with DNNs, termed DNN U-learning, which is detailed in Algorithm 2.

3 Theoretical Properties

3.1 Lasso U-learning

We will show that the U-learning prediction (6) is consistent and asymptotically normal, as well as the consistency of the variance estimator (7). We start by stating the *Restricted Eigenvalue (RE)* condition which is commonly used in the Lasso literature and will be used

Algorithm 2 DNN U-learning prediction and inference

Require: DNN architecture (L, \mathbf{p}) , subsample size $r < n$, number of subsamples B

Input: Training data \mathcal{T}_n , a test point \mathbf{x}_*

Output: Prediction \hat{y}_*^B and $100(1 - \alpha)\%$ confidence interval $(\hat{L}(\mathbf{x}_*), \hat{U}(\mathbf{x}_*))$

- 1: **for** $j = 1, 2, \dots, B$ **do**
 - 2: Random subsample data of size r without replacement. Denote by \mathcal{T}^{b_j} the resampled data (indexed by \mathcal{I}^{b_j}), and save the sampling vector $\mathbf{J}_{b_j} = (J_{b_j,1}, \dots, J_{b_j,n})$
 - 3: Fit DNN(L, \mathbf{p}) on \mathcal{T}^{b_j} with $\mathcal{T} \setminus \mathcal{T}^{b_j}$ as the validation set
 - 4: Denote the fitted model as \tilde{f}^{b_j}
 - 5: **end for**
 - 6: Compute $\hat{y}_*^B = \frac{1}{B} \sum_{j=1}^B \tilde{f}^{b_j}(\mathbf{x}_*)$ and $\hat{\sigma}_*^2$ by (7)
 - 7: Compute the confidence interval for $f_0(\mathbf{x}_*)$ as $(\hat{y}_*^B - z_{1-\alpha/2}\hat{\sigma}_*, \hat{y}_*^B + z_{1-\alpha/2}\hat{\sigma}_*)$
-

for formulating our regularity conditions. Given a set $S \subseteq \{1, 2, \dots, p\}$ and a positive number c_α , \mathbf{X} is said to satisfy the RE condition if there exists a constant $\kappa > 0$ such that for all vectors $\Delta \in \mathbb{R}^p$ satisfying $\|\Delta_{S^c}\|_1 \leq c_\alpha \|\Delta_S\|_1$, it holds that $\frac{1}{n} \|\mathbf{X}\Delta\|_2^2 \geq \kappa \|\Delta\|_2^2$. The RE condition essentially controls multicollinearity among the predictors, and the eigenvalues of submatrices of $\mathbf{X}^T \mathbf{X}$. As such, we state the following conditions required for our theorems.

- (C1) The errors ε_i 's are independent of \mathbf{x}_i 's and i.i.d. with mean zero and a finite variance σ_ε^2 . Further, there exists a constant $M > 0$, such that $\|\mathbf{x}_i\|_\infty < M$ almost surely for all i . The design matrix \mathbf{X} satisfies the RE condition with constants $(\kappa, 3)$.
- (C2) The subsampling size r_n satisfies $\lim_{n \rightarrow \infty} r_n = \infty$ and $\lim_{n \rightarrow \infty} r_n \log(p)/n = 0$. (In the ensuing theoretical development, we introduce a subscript n to r to emphasize its reliance on the sample size n .)
- (C3) There exists a constant K_0 , such that $|\beta^0|_1 = \sum_{j=1}^p |\beta_j^0| < K_0$. Let $\{K_n\}_{n \geq 1}$ be a sequence of constants satisfying $K_n > K_0$ for the Lasso problem (3), where given the training set, the same K_n is used to fit (3) on all subsamples $\mathcal{T}^b, b = 1, 2, \dots, B$.

Condition (C1) is standard in restricting the input covariates of the true model. Condition (C2) stipulates the relationship between the the order of r_n, n and p . Condition (C3) is needed for the prediction consistency of Lasso and ensures that there is no additional randomness in fitting the Lasso on \mathcal{T}^b . Moreover, diverging from the conventional high-dimensional literature, we do not impose sparsity on the coefficient vector β^0 , as our focus is on predictive inference rather than drawing inferences about individual effects. We first present a result on prediction consistency of Lasso (Chatterjee, 2013).

Lemma 1 *Under (C1), and for $K_n > K_0$ as defined in (C3), the prediction \hat{y}_*^b based on (3) satisfies*

$$\mathbb{E} \left[(\hat{y}_*^b - f_0(\mathbf{x}_*))^2 \right] \leq 2K_n M \sigma_\varepsilon \sqrt{\frac{2 \log(2p)}{n}} + 8K_n^2 M^2 \sqrt{\frac{2 \log(2p^2)}{n}}.$$

Remark: To ensure the consistency of the ensemble prediction, the Lemma establishes the prediction consistency for each subsample under conditions much weaker than for the

“estimation consistency.” For example, Lasso yields shrinkage coefficient estimators that are biased and require stringent conditions for consistent estimates or model selection (Zhao and Yu, 2006; Chatterjee and Lahiri, 2011); in contrast, Lasso prediction consistency can be readily obtained from past works with much weaker assumptions (Chatterjee, 2013; Bartlett et al., 2012; Rigollet and Tsybakov, 2011; Bühlmann and Van De Geer, 2011).

Extending the discussion of the variance of a U-statistic in Hoeffding (1992), we define

$$\xi_{1,r_n}(\mathbf{x}_*) = \text{Cov} \left(\tilde{f}(\mathbf{x}_*; Z_1, Z_2, \dots, Z_{r_n}), \tilde{f}(\mathbf{x}_*; Z_1, Z_2', \dots, Z_{r_n}') \right)$$

as the covariance of the Lasso predictions (4) on two subsamples with one sample in common. Because the data points Z_i, Z_i' 's follow the same data generation process, and given that both predictions are asymptotically consistent, it would be reasonable to assume $\liminf \xi_{1,r_n}(\mathbf{x}_*) > 0$. As such, we present the first main result on the asymptotic normality of the Lasso U-learning prediction.

Theorem 2 *Given the training data $\mathcal{T}_n = \{Z_i = (y_i, \mathbf{x}_i) : 1 \leq i \leq n\}$ drawn from model (2) and a fixed \mathbf{x}_* in the support of \mathcal{X} , the distribution generating \mathbf{x}_i , let $\hat{y}_*^B = \hat{f}^B(\mathbf{x}_*)$ be the U-learning prediction defined as in (6) and Algorithm 1. Then under (C1) - (C3), as $n \rightarrow \infty$ and $n/B \rightarrow 0$,*

i)

$$\frac{\sqrt{n} (\hat{y}_*^B - f_0(\mathbf{x}_*))}{v_n(\mathbf{x}_*)} \xrightarrow{d} N(0, 1)$$

$$\text{where } v_n(\mathbf{x}_*) = \sqrt{r_n^2 \xi_{1,r_n}(\mathbf{x}_*)}.$$

ii) $n\hat{\sigma}_*^2/v_n^2 \xrightarrow{p} 1$.

Theorem 2 establishes the asymptotic normality of the U-learning prediction \hat{y}_*^B and the consistency of the infinitesimal jackknife variance estimator $\hat{\sigma}_*^2$. These results form the foundation for conducting statistical inference. The key advantage of employing the infinitesimal jackknife approach lies in that we do not need to compute or estimate $v_n(\mathbf{x}_*)$ or $\xi_{1,r_n}(\mathbf{x}_*)$ analytically; instead, we can compute its asymptotic equivalence $\hat{\sigma}_*^2$, which is embedded in the resampling scheme. Also, when proving this theorem, we show and use the asymptotic normality of the Hájek projection of \hat{y}_*^B ; see the Appendix. The asymptotic normality ensures valid construction of confidence intervals for future predictions, as stated in the Corollary.

Corollary 3 *Under the same setting as in Theorem 2, and with $\hat{\sigma}_*^2$ defined in (7), the following confidence interval is asymptotically valid with a target probability of $1 - \alpha$ ($0 < \alpha < 1$). That is, as $n \rightarrow \infty$, $\Pr \left[f_0(\mathbf{x}_*) \in \left(\hat{L}(\mathbf{x}_*), \hat{U}(\mathbf{x}_*) \right) \right] \rightarrow 1 - \alpha$, where*

$$\hat{L}(\mathbf{x}_*) = \hat{y}_*^B - z_{1-\alpha/2} \hat{\sigma}_*, \quad \hat{U}(\mathbf{x}_*) = \hat{y}_*^B + z_{1-\alpha/2} \hat{\sigma}_*,$$

and $z_{1-\alpha/2}$ is the $(1 - \alpha/2)$ -th quantile of the standard normal distribution.

3.2 DNN U-learning

Since the Universal Approximation Theorem (Hornik et al., 1989), much work has been accomplished on the prediction accuracy and rate of convergence of neural networks; see McCaffrey and Gallant (1994); Bolcskei et al. (2019); Schmidt-Hieber (2020), among many others. The performance of a DNN is typically measured by the bound on the prediction error,

$$R(\widehat{f}_n, f_0) = \mathbb{E}_{f_0} \left[\left(\widehat{f}_n(\mathbf{x}_*) - f_0(\mathbf{x}_*) \right)^2 \right],$$

where \widehat{f}_n is the DNN estimator based on the training set \mathcal{T}_n , \mathbb{E}_{f_0} indicates that the expectation is taken under the true function f_0 under model (1), and \mathbf{x}_* is a fixed testing point. While the rate of convergence would vary depending on different model assumptions and DNN architectures, various previous works have provided results on the prediction consistency. For example, McCaffrey and Gallant (1994) on shallow neural networks (one hidden layer) has derived a convergence rate of $n^{-2\gamma/(2\gamma+p+5)}$, where γ is the smoothness parameter and p is the number of covariates. Additional insights for multilayer neural networks can be found in Kohler and Krzyżak (2005), which achieves the nonparametric rate $n^{-2\gamma/(2\gamma+p)}$ for γ -smooth functions f_0 and $\gamma \leq 1$ with two-layer NNs using the sigmoid activation function. Extensions of this work include Bauer and Kohler (2019); Kohler and Langer (2021).

In order to derive the convergence rate of $\widehat{f}_n \in \mathcal{F}(L, \mathbf{p})$ [defined underneath (8)], we first introduce

$$\Delta_n(\widehat{f}_n, f_0) = \mathbb{E}_{f_0} \left[\frac{1}{n} \sum_{i=1}^n \left(y_i - \widehat{f}_n(\mathbf{x}_i) \right)^2 - \inf_{f \in \mathcal{F}(L, \mathbf{p})} \frac{1}{n} \sum_{i=1}^n \left(y_i - f(\mathbf{x}_i) \right)^2 \right].$$

The sequence $\Delta_n(\widehat{f}_n, f_0)$ measures the difference between the expected empirical risk of \widehat{f}_n and the global minimum over all networks in the class. Therefore, $\Delta_n(\widehat{f}_n, f_0) = 0$ if \widehat{f}_n is an empirical risk minimizer. For the theoretical derivations, we refer to the framework established by Schmidt-Hieber (2020), which assumes $f_0 = g_q \circ g_{q-1} \circ \dots \circ g_1 \circ g_0$ with $g_i : [a_i, b_i]^{d_i} \rightarrow [a_{i+1}, b_{i+1}]^{d_{i+1}}$. Denote by $g_i = (g_{ij})_{j=1, \dots, d_{i+1}}^T$ the components of g_i , and let t_i be the maximal number of variables on which each of the g_{ij} depends on. Thus, each g_{ij} is a t_i -variate function. We assume that each of the functions g_{ij} has Hölder smoothness γ_i , denoted by $g_{ij} \in C_{t_i}^{\gamma_i}([a_i, b_i]^{d_i})$. Since g_{ij} is also t_i -variate, $g_{ij} \in C_{t_i}^{\gamma_i}([a_i, b_i]^{t_i})$, and the underlying function space is

$$\mathcal{G}(q, \mathbf{d}, \mathbf{t}, \boldsymbol{\gamma}, K) := \left\{ f = g_q \circ \dots \circ g_0 : g_i = (g_{ij})_j : [a_i, b_i]^{d_i} \rightarrow [a_{i+1}, b_{i+1}]^{d_{i+1}}, \right. \\ \left. g_{ij} \in C_{t_i}^{\gamma_i}([a_i, b_i]^{t_i}) \text{ with } |a_i|, |b_i| \leq K \right\},$$

with $\mathbf{d} := (d_0, \dots, d_{q+1})$, $\mathbf{t} := (t_0, \dots, t_q)$, $\boldsymbol{\gamma} := (\gamma_0, \dots, \gamma_q)$. Further define the effective smoothness indices as $\gamma_i^* := \gamma_i \prod_{\ell=i+1}^q (\gamma_\ell \wedge 1)$, and $\phi_n := \max_{i=0, \dots, q} n^{-\frac{2\gamma_i^*}{2\gamma_i^* + t_i}}$. Lastly, to facilitate our ensuing theoretical development, we focus on a class of s -sparse and F -bounded networks, defined as

$$\mathcal{F}(L, \mathbf{p}, s, F) := \left\{ f \in \mathcal{F}(L, \mathbf{p}) : \sum_{j=0}^L \|\mathbf{w}_j\|_0 \leq s, \|f\|_\infty \leq F \right\}.$$

We require the following conditions.

- (D1) The input features \mathbf{x} are bounded between $[0, 1]$.
- (D2) The subsampling size r_n satisfies $\lim_{n \rightarrow \infty} r_n = \infty$ and $\lim_{n \rightarrow \infty} r_n \log(p)/n = 0$.
- (D3) $\widehat{f}_n \in \mathcal{F}(L, \mathbf{p}, s, F)$ with L , \mathbf{p} and s satisfying
- (i) $\sum_{i=0}^q \log_2(4t_i \vee 4\gamma_i) \log_2 n \leq L \lesssim \log^\alpha n$ where $\alpha > 1$,
 - (ii) $n\phi_n \lesssim \min_{i=1, \dots, L} p_i$,
 - (iii) $s \asymp n\phi_n \log n$,

where $a_n \lesssim b_n$ means there exists a constant $C > 0$ such that $0 < a_n \leq Cb_n$ when n is sufficiently large, and $a_n \asymp b_n$ means both $a_n \lesssim b_n$ and $b_n \lesssim a_n$ hold.

- (D4) There exists a constant C such that the expected empirical risk difference $\Delta_n(\widehat{f}_n, f_0) \leq C\phi_n L \log^2 n$.

Conditions (D1) and (D2) are analogous to (C1) and (C2). Condition (D3) specifies the requirements on the network parameters relative to the sample size and smoothness parameters ϕ_n, t_i, γ_i , including the number of layers L , the boundness parameter F , and the sparsity s . Note that s is allowed to increase with n , and in practice we can apply regularization and dropout layers in applications to control the network sparsity. The boundness of network is a technical condition, ensuring the convergence of DNN U-learning predictions. Condition (D4) assumes that we could obtain a fit \widehat{f}_n that is “close enough” to the global minimum within the class of neural networks. Combining (D3) and (D4) leads to the consistency requirement on the neural network, as we re-write Theorem 1 of Schmidt-Hieber (2020) as a lemma below, giving the convergence rate of \widehat{f}_n essential for deriving the prediction inference properties.

Lemma 4 *Consider Model (1) and f_0 in the class $\mathcal{G}(q, \mathbf{d}, \mathbf{t}, \gamma, K)$. Let \widehat{f}_n be an estimator in the neural network class $\mathcal{F}(L, \mathbf{p}, s, F)$. If conditions (D3) and (D4) are satisfied, there exist constants $0 < c^* < 1/2$ and C' such that $\phi_n = o(n^{-c^*})$, and*

$$R(\widehat{f}_n, f_0) \leq C' \phi_n L \log^2 n.$$

Lemma 4 establishes the bound of prediction errors within the class $\mathcal{F}(L, \mathbf{p}, s, F)$, where c^* is determined by the smoothness of f_0 . In contrast to Theorem 2 for Lasso U-learning, deriving the asymptotics for DNN U-learning predictors introduces a key distinction: while Lasso solutions are uniquely determined by data and the regularization parameter K_n , fitting NNs introduces additional randomness through gradient-based algorithms. Consequently, adjustments to the proof are necessary, akin to the modifications outlined in Theorem 2 of Mentch and Hooker (2016). Let ω denote the randomness involved in fitting a DNN, such as shuffling in batches, or the randomness in stochastic gradient descent (SGD) or other optimization algorithms, which leads to a nuanced formulation:

$$\begin{aligned} \widetilde{f}^{b_j}(\mathbf{x}_*) &= \widetilde{f}^{(\omega_j)}(\mathbf{x}_* | L, \mathbf{p}, \mathcal{T}^{b_j}), \\ \widehat{y}_*^B &= \frac{1}{B} \sum_{j=1}^B \widetilde{f}^{b_j}(\mathbf{x}_*) = \frac{1}{B} \sum_{j=1}^B \widetilde{f}^{(\omega_j)}(\mathbf{x}_* | L, \mathbf{p}, \mathcal{T}^{b_j}), \end{aligned}$$

where $\omega_1, \dots, \omega_B \sim_{i.i.d.} F_\omega$, and are independent of the observations \mathcal{T}_n . As specified in Algorithm 2, we apply a fixed architecture (L, \mathbf{p}) to all subsamples. The resulting ensemble prediction is asymptotically normal after applying Lemma 4.

Theorem 5 *Suppose that the training data $\mathcal{T}_n = \{Z_i = (y_i, \mathbf{x}_i) : 1 \leq i \leq n\}$ are generated from model (1) with an unknown f_0 , and \mathbf{x}_* is a fixed testing point that lies in the support of \mathcal{X} . Assume the neural network fit on subsamples in Algorithm 2 belongs to $\mathcal{F}(L, \mathbf{p}, s, F)$ and satisfies (D4) for the subsample size r_n . In addition, (D1) – (D3) hold, as well as $\liminf \xi_{1,r_n}(\mathbf{x}_*) > 0$ and $\forall j$*

$$\lim_{n \rightarrow \infty} \mathbb{E} \left(\tilde{f}^{(\omega_j)}(\mathbf{x}_* | \mathcal{T}^{b_j}) - \mathbb{E}_\omega \tilde{f}^{(\omega_j)}(\mathbf{x}_* | \mathcal{T}^{b_j}) \right)^2 < \infty, \quad (9)$$

where \mathbb{E}_ω is the expectation taken over F_ω . Then the U-learning prediction by Algorithm 2 satisfies, as $n \rightarrow \infty, n/B \rightarrow 0$,

$$\frac{\sqrt{n} (\hat{y}_*^B - f_0(\mathbf{x}_*))}{v_n(\mathbf{x}_*)} \xrightarrow{d} N(0, 1)$$

for $v_n = \sqrt{r_n^2 \xi_{1,r_n}(\mathbf{x}_*)}$.

Remark: The additional Condition (9), an analog to that in Mentch and Hooker (2016), prevents the randomness, when fitting a DNN on a subsample dataset, from causing much difference among predictions from the same subsample as $n \rightarrow \infty$, and eventually controls the difference between \hat{y}_*^B and its non-random counterpart.

Because the analytic form of ξ_{1,r_n} is unavailable, we estimate the variances via infinitesimal jackknife. Recall $\hat{\sigma}_*^2$ as defined in (7). The following corollary explicitly writes out the confidence interval for predictions with NNs. The proof is omitted due to its similarity with the proof of Corollary 3.

Corollary 6 *Under the same setting as in Theorem 5, the following confidence interval is asymptotically valid with a target probability of $1 - \alpha$ ($0 < \alpha < 1$). That is, as $n \rightarrow \infty$, $\Pr \left[f_0(\mathbf{x}_*) \in \left(\hat{L}(\mathbf{x}_*), \hat{U}(\mathbf{x}_*) \right) \right] \rightarrow 1 - \alpha$, where*

$$\hat{L}(\mathbf{x}_*) = \hat{y}_*^B - z_{1-\alpha/2} \hat{\sigma}_*, \quad \hat{U}(\mathbf{x}_*) = \hat{y}_*^B + z_{1-\alpha/2} \hat{\sigma}_*,$$

and $z_{1-\alpha/2}$ is the $(1 - \alpha/2)$ -th quantile of the standard normal distribution.

4 Numerical Experiments

We conduct numerical experiments to assess the finite-sample performance of the proposed U-learning methods and compare them with an Oracle estimator (assuming the true active set known) and the conformal prediction interval (Chernozhukov et al., 2021). We consider three examples: i) high dimensional linear models with the Lasso; ii) non-linear models with neural networks; iii) WHO Life Expectancy Data, a public dataset for training and evaluating neural networks. In each example, we randomly split the data into the training and testing sets, fit the model on the training set, and assess the prediction performance on the testing set via the average bias and mean absolute error (MAE) between the truth

and the predicted values, i.e., for ℓ testing samples, $MAE = \frac{1}{\ell} \sum_{\ell=1}^{\ell} |f_0(\mathbf{x}_\ell) - \hat{f}^B(\mathbf{x}_\ell)|$. We further report the average interval length (AIL), i.e., $\frac{1}{\ell} \sum_{\ell=1}^{\ell} (U_\ell - L_\ell)$, and the coverage probability (CP), i.e., $\frac{1}{\ell} \sum_{\ell=1}^{\ell} I(f_0(\mathbf{x}_\ell) \in [\hat{L}_\ell, \hat{U}_\ell])$. In the third example, we replace $f_0(\mathbf{x}_\ell)$ by the corresponding observed value as an approximation without knowing the “truth.”

Example 1 (Lasso U-learning with high dimensional linear truth). To mimic the real-world DNA methylation data, we let $p = 3000$, with $s_0 = 25$ non-zero signals taking values between -1 and 1.5 . We ran two scenarios with training sizes $n = 500$ and $n = 1000$, respectively, and one fixed testing set with sample size $\ell = 200$. Two hundred training sets were simulated following the linear model (2). To implement the proposed algorithm, we chose K by 5-fold cross validation on the entire training set, used $B = 500$ and subsampling with $r = n^\gamma$ for $\gamma = 0.8, 0.9$ and 0.95 . The oracle estimates of prediction and CIP were derived assuming the true active set was known, and the model was fit in each subsample in Algorithm 1 instead of the Lasso. For comparison, we implemented the approach of sampling with replacement (SWR, i.e., we replaced subsamples with bootstrap samples of size $r = n$ in Algorithm 1), the naive bootstrap approach (prediction using the entire training set, while using B bootstrap resamples to derive the prediction SEs and confidence intervals based on normal approximation), and the conformal prediction (Lei et al., 2018).

Table 1 summarizes the results, highlighting several key observations. First, as expected, the oracle method presents the narrowest confidence intervals. Second, concerning the proposed U-learning approach, the average bias, MAE, and Standard Error (SE) in prediction exhibit variability with respect to the subsample size r , achieving optimal results at $r = n^{0.9}$ and $r = n^{0.95}$. Third, the performance of U-learning improves notably as the sample size n increases from 500 to 1000, with computed SE values approaching empirical standard deviations and coverage probabilities of confidence intervals aligning more closely with the 0.95 nominal level. Particularly, at $n = 1000$ and with $r = n^{0.9}$ or $r = n^{0.95}$, its AIL (0.436 or 0.441) is comparable to that of the Oracle (0.360). Additionally, Figure 1 depicts the average coverage probability on the test samples (panels a, c) and the average prediction SEs (panels b, d) in both scenarios. The empirical coverage probability is close to the nominal coverage probability. Our approach can also effectively capture individual variation in prediction, as evidenced by the varying SE values. Fourth, it is noteworthy that the SEs of the two bootstrap methods (SWR and naive) fail to match the empirical standard deviations and nominal coverage level even as the sample size increases. This is because the SWR variant does not fit the generalized U-statistic framework and the Naive Bootstrap does not yield asymptotically normal predictions. Finally, for a fair comparison, we slightly modified conformal prediction by using the true $f_0(\mathbf{x}_*)$ instead of y_* when deriving the conformity score. Nevertheless, we find that, while conformal prediction intervals (PIs) yield comparable coverage probabilities, it is less efficient with much larger AIL. In terms of computation, the U-learning computation time is proportional to the training sample size n and B . Empirically on an 8-core CPU machine with parallel computing, the average run time per training set is 88 seconds for $n = 500$ and 272 seconds for $n = 1000$.

Example 2 (DNN U-learning with non-linear truth). We considered the following scenarios of non-linear truth,

$$\text{Scenario 1: } f_0(\mathbf{x}) = -\sin(\pi x_1) + 2(x_2 - 0.5)^2 + 1.5x_3x_4 - \frac{5}{x_5}, \quad x_j \sim \text{Unif}(1, 2);$$

$$\text{Scenario 2: } f_0(\mathbf{x}) = 0.5x_1^2 - 0.3x_5x_{10} + e^{0.2x_{15}} + \cos x_{20}, \quad \mathbf{x} \sim N(\mathbf{0}, \Sigma),$$

with a total of $p = 100$ covariates and $\Sigma = (0.5^{|j-k|})_{j,k=1,\dots,p}$. In each scenario, we simulated 200 training sets with varying subsample sizes r from $n^{0.8}$ to $n^{0.95}$, for $n = 200$ and 600 , and a fixed test set of 100 samples. We applied the DNN U-learning algorithm with a network structure of $L = 2$ and layer dimensions defined by $\mathbf{p} = (p, 128, 64, 1)$. Each hidden dense layer is also followed by a dropout layer with a 50% dropout rate for regularization. We set $B = 300$. For comparisons, we also applied conformal prediction based on 600 training samples. Table 2 summarizes the results obtained for each combination of n and r . In each scenario, the r values that yield the coverage probability closest to 95% are highlighted in bold. As n increases, the mean bias, MAE, prediction SE and AIL tend to decrease. Both choices of r , $r = n^{0.9}$ and $r = n^{0.95}$, result in improved coverage probability (CP) and narrower AIL compared to $r = n^{0.8}$, while the computational times remain comparable across all three scenarios. With n increasing, the prediction SE aligns more closely with the empirical SD, and both decrease gradually, leading to more efficient CIs with coverage probability closer to the nominal level. Again, conformal PIs are derived by using the true $f_0(\mathbf{x}_*)$ in lieu of y_* for a fair comparison. Their prediction intervals generally exhibit wider widths and larger AILs, with coverage probabilities exceeding the nominal level, indicating underperformance compared to our proposed method. The U-learning method was implemented on a computing cluster with 30 CPU cores, which parallelized the subsampling scheme. This parallelization reduces computation time compared to running the algorithm on a single core.

Example 3 (WHO Life Expectancy Data). As a real data example, we analyzed a publicly available life expectancy dataset collected by WHO during 2000 to 2015 for the majority of countries in the world (Kumarajarshi, 2023). Features in the model included important immunizations like Hepatitis B, Polio and Diphtheria and mortality factors, economic factors, social factors and other health related factors ($p = 20$). Due to the dependency between the years of the same country, regression models for i.i.d. samples were not suitable, and we opted to use Algorithm 2 with DNN U-learning. We randomly split the data into the training and testing sets ($n = 1319$, $\ell = 330$), and applied the proposed approach with a DNN with 3 hidden layers and $\mathbf{p} = (20, 64, 128, 32, 1)$. With $B = 1500$, we provided the prediction and inference in panel (a) of Figure 2.

The confidence intervals that did not cover the true life expectancy were highlighted in black, with an empirical coverage probability of 0.967 in all testing samples. The average bias was -0.12 years and an MAE of 2.2 years. The AIL was 16.2 years. There were a total of 9 countries whose PIs did not cover the actual life expectancies, including Bangladesh, Belarus, China, India, Mozambique, among others. Noticeably, all of them were developing countries, except for Romania (Figure 2a). Notably, the country exhibiting the most substantial prediction bias, India, where the predicted life expectancy surpasses 100, also displayed a wide confidence interval, albeit not encompassing the observed life expectancy. In contrast, the conformal prediction approach yielded an average bias of -0.98 and Mean

Absolute Error (MAE) of 2.6 years, accompanied by confidence intervals with a consistent length of 16.9 years across all countries. These intervals maintained an average coverage probability of 0.942 at the population level, yet they did not capture the individual variability within each country (Figure 2b). It is noted that our approach outperformed the conformal prediction method in terms of covering countries with extreme life expectancies. For instance, the intervals obtained by using the proposed approach effectively covered countries like Malawi with the lowest life expectancy, as well as countries such as France, Germany, and Belgium with the highest life expectancies.

5 Epigenetic Clocks with Human Methylation Data Across Multiple Tissues

The aging process is linked to methylation levels at specific individual CpG sites and is collectively associated with subsets of CpGs (Lin et al., 2016). DNA methylation clocks, also known as epigenetic aging clocks, have been developed (Horvath, 2013; Bell et al., 2019; Yu et al., 2020). These clocks employ multi-predictor regression models based on sets of CpG sites to predict the methylation age of subjects. The methylation age demonstrates correlation with observed chronological age and holds potential for quantifying biological aging rates, as well as evaluating longevity or rejuvenating interventions (Marioni et al., 2015; Lu et al., 2019).

There is a lack of uncertainty measures associated with epigenetic aging clocks. This challenge motivated us to incorporate prediction and inference methods in the development of these clocks. We compiled DNA methylation data from individuals covering a wide age spectrum, ranging from 8 to 101 years old. Methylation levels were evaluated at more than 37,000 CpG sites spanning the entire human genome. Our dataset encompasses 522 blood samples and 781 non-blood samples from diverse tissue types, such as lung, liver, kidney, heart, and others. The samples comprise of healthy individuals, as well as those with various health conditions (Table 4). In the following, we present comprehensive analyses with both Lasso U-learning and DNN U-learning approaches, and explore modeling the blood and non-blood samples separately or jointly.

To assess model performance and address data heterogeneity, we started by applying Lasso U-learning separately to blood samples and non-blood samples. Let $B = 3000$, and the subsample size $r = n^{0.95}$. We utilized “out-of-bag” (OOB) estimates to obtain unbiased predictions for all samples. For each subsample b , DNAmAge was predicted solely on its complement set. The performance of the two U-learning clocks concerning blood samples and non-blood samples is summarized in Figure 3 and Table 3 (first two columns). Both clocks exhibit accuracy in terms of bias (-0.01 vs. 0.04) and correlation (0.99 versus 0.93) between predicted DNAmAge and chronological age. The notable distinction lies in the blood clock providing more accurate predictions with smaller variances, evident in the error bars and the comparison of standard errors (SE) in the Figure. Traditional aging clocks, lacking robust measures of uncertainty, might overlook such differences between homogeneous and heterogeneous samples without these new tools for prediction inference.

To compare Lasso U-learning and DNN U-learning, we further analyzed the dataset by randomly splitting the total 1303 samples into 1000 training samples and 303 testing samples. Implementing Algorithm 2, we performed screening on the training data, reducing

it to 2905 CpG sites in addition to the 13 tissue indicators. Hyperparameter search involved exploring the number of hidden layers L , the numbers of neurons \mathbf{p} , and the learning rate. The final model selected was a 1-hidden-layer NN with $L = 3$, $\mathbf{p} = (2918, 256, 1)$, and the hidden layer was followed by a dropout layer with a 0.5 dropout rate.

As indicated in columns 3 and 4 of Table 3, the DNN U-learning clock exhibited a lower Mean Absolute Error (MAE) and comparable bias to the Lasso U-learn clock. The average prediction variances were slightly larger for DNN U-learning compared to those from Lasso-based inference. The prediction variances by DNN U-learning displayed less variability than those by Lasso U-learning, yet both achieved the same coverage probability of $ACIL = 0.954$.

Overall, U-learning with both Lasso and NN resulted in comparable predictions and confidence intervals (Table 4, Figure 4). The majority of the samples not covered were from non-blood tissues, with 2 out of 120 blood samples and 12 out of 183 non-blood samples not covered by DNN U-learning (Figure 4a). Similarly, 1 blood sample and 13 non-blood samples had ages not covered by the PIs from Lasso U-learning (Figure 4b). This suggested that age prediction in non-blood samples was more variable, possibly due to un-captured variability arising from the smaller number of samples per tissue.

We also examined the U-learning PIs’ coverage across various health conditions of individuals, as detailed in Table 4. Patients were categorized based on their primary diagnoses, including Healthy, Alzheimer’s Disease, Other Neuro-degenerative Diseases (OtherBrain), HIV, Chronic Diseases (ChronCond), and Parkinson’s Disease. For all 72 healthy individuals, the PIs covered their chronological ages, affirming the accuracy of DNAmAges and the reliability of inferences derived from our method. In comparison to the healthy group, the proportions of PI coverage in other disease groups were similar, except for Alzheimer’s Disease, where 4 out of 11 individuals exhibit non-covered PIs. Notably, the DNAmAges of these 4 individuals significantly surpassed their chronological ages, with a mean difference of 11.6 years. This outcome provided additional confirmation of the connection between DNA methylation and Alzheimer’s Disease, consistent with findings reported in recent studies (McCartney et al., 2018; Sugden et al., 2022; Milicic et al., 2023).

In summary, our analysis offered a new perspective by pinpointing individuals whose ages notably deviated from their predicted DNAmAges. Subsequent experiments may delve into the underlying biological differences among these individuals, paving the way for further exploration and understanding.

6 Conclusions

We have proposed a U-learning procedure for valid prediction inference that can be applied to high-dimensional linear regressions with Lasso, as well as non-parametric machine learning algorithms like the multi-layer neural networks. The inference and confidence intervals are subject-specific that estimate the prediction variance conditional on each future sample. The theoretical properties are derived based on generalized U-statistics and Hájek projections. We have illustrated the methods by comparison with conformal predictions in several numerical examples. A comprehensive real data analysis of a large scale DNA methylation study on human aging was presented, resulting in novel epigenetic clocks with valid confidence intervals that can quantify the uncertainty in predictions.

A natural extension of the proposed method is to the classification problems that involve binary or multi-class outcomes. We envision that the generalized U-statistic techniques can be updated to suit the problems. Future research is also warranted in further improving the computational efficiency of the U-learning methods, especially in the context of neural networks. This may be achieved by exploring the network architectures, i.e., (L, \mathbf{p}) , and modifications to the optimization algorithms. For example, theoretical investigation of dropout layers in place of the subsampling scheme to incorporate ensemble within the training of one NN. Nevertheless, this work lays the foundation towards valid inferences with deep learning models and unveiling their black box nature.

We may further derive *prediction intervals* for the unobserved y_* , which requires estimation of the error distribution; see the related literature on conformal predictions (Papadopoulos, 2008; Lei et al., 2018; Messoudi et al., 2020). Consider a specific extension when the errors are i.i.d. normally distributed. With $\Delta_* = y_* - \hat{f}(\mathbf{x}_*)$, note that

$$\Delta_* = \left(f_0(\mathbf{x}_*) - \hat{f}(\mathbf{x}_*) \right) + \varepsilon_*$$

leads to

$$\text{Var}(\Delta_*) = \sigma_*^2 + \sigma_\varepsilon^2,$$

as ε_* is independent of $\{f_0(\mathbf{x}_*) - \hat{f}(\mathbf{x}_*)\}$. The first term on the right hand side reflects the model uncertainty, and is subject-dependent, while the second term is the random *error variance* attached to all observations. We will pursue this in future works.

Acknowledgements

This work is partially supported by NIH grants. We are grateful toward Dr. Steve Horvath for providing the DNA Methylation data from the Mammalian Methylation Consortium and insightful discussions.

References

- Anders Andreassen and Ethan Dyer. Asymptotics of wide convolutional neural networks. *arXiv preprint arXiv:2008.08675*, 2020.
- Anastasios N Angelopoulos and Stephen Bates. A gentle introduction to conformal prediction and distribution-free uncertainty quantification. *arXiv preprint arXiv:2107.07511*, 2021.
- Susan Athey, Guido W Imbens, and Stefan Wager. Approximate residual balancing: de-biased inference of average treatment effects in high dimensions. *Journal of the Royal Statistical Society: Series B (Statistical Methodology)*, 80(4):597–623, 2018.
- Vahe Avagyan and Stijn Vansteelandt. High-dimensional inference for the average treatment effect under model misspecification using penalized bias-reduced double-robust estimation. *Biostatistics & Epidemiology*, 6(2):221–238, 2022.
- Rina Foygel Barber, Emmanuel J. Candès, Aaditya Ramdas, and Ryan J. Tibshirani. Predictive inference with the jackknife+. *Ann. Statist.*, 49(1):486–507, Feb 2021. doi: 10.1214/20-AOS1965.

- Peter L Bartlett, Shahar Mendelson, and Joseph Neeman. ℓ_1 - regularized linear regression: persistence and oracle inequalities. *Probability theory and related fields*, 154(1):193–224, 2012.
- Benedikt Bauer and Michael Kohler. On deep learning as a remedy for the curse of dimensionality in nonparametric regression. *The Annals of Statistics*, 47(4):2261–2285, August 2019. doi: 10.1214/18-AOS1747.
- Christopher G Bell, Robert Lowe, Peter D Adams, Andrea A Baccarelli, Stephan Beck, Jordana T Bell, Brock C Christensen, Vadim N Gladyshev, Bastiaan T Heijmans, Steve Horvath, et al. Dna methylation aging clocks: challenges and recommendations. *Genome biology*, 20:1–24, 2019.
- Alexandre Belloni, Victor Chernozhukov, and Christian Hansen. High-dimensional methods and inference on structural and treatment effects. *Journal of Economic Perspectives*, 28(2):29–50, 2014a.
- Alexandre Belloni, Victor Chernozhukov, and Christian Hansen. Inference on treatment effects after selection among high-dimensional controls. *The Review of Economic Studies*, 81(2):608–650, 2014b.
- Alexandre Belloni, Victor Chernozhukov, and Ying Wei. Post-selection inference for generalized linear models with many controls. *Journal of Business & Economic Statistics*, 34(4):606–619, 2016.
- Helmut Bolcskei, Philipp Grohs, Gitta Kutyniok, and Philipp Petersen. Optimal approximation with sparsely connected deep neural networks. *SIAM Journal on Mathematics of Data Science*, 1(1):8–45, 2019.
- Jelena Bradic, Weijie Ji, and Yuqian Zhang. High-dimensional inference for dynamic treatment effects. *arXiv preprint arXiv:2110.04924*, 2021.
- Peter Bühlmann and Sara Van De Geer. *Statistics for high-dimensional data: methods, theory and applications*. Springer Science & Business Media, 2011.
- A Chatterjee and SN Lahiri. Strong consistency of lasso estimators. *Sankhya A*, 73:55–78, 2011.
- Sourav Chatterjee. Assumptionless consistency of the lasso. *arXiv preprint arXiv:1303.5817*, 2013.
- Victor Chernozhukov, Kaspar Wüthrich, and Yinchu Zhu. Distributional conformal prediction. *Proceedings of the National Academy of Sciences*, 118(48):e2107794118, 2021.
- Bradley Efron and Charles Stein. The jackknife estimate of variance. *The Annals of Statistics*, 9(3):586–596, 1981.
- Zhe Fei and Yi Li. Estimation and inference for high dimensional generalized linear models: A splitting and smoothing approach. *Journal of Machine Learning Research*, 22(58):1–32, 2021.

- Zhe Fei, Ji Zhu, Moulinath Banerjee, and Yi Li. Drawing inferences for high-dimensional linear models: A selection-assisted partial regression and smoothing approach. *Biometrics*, 75(2):551–561, 2019.
- Zhe Fei, Qi Zheng, Hyokyoung G Hong, and Yi Li. Inference for high-dimensional censored quantile regression. *Journal of the American Statistical Association*, 118(542):898–912, 2023. PMID: not yet available.
- Edward W Frees. Infinite order u-statistics. *Scandinavian Journal of Statistics*, 16(1):29–45, 1989.
- Wenjiang Fu and Keith Knight. Asymptotics for lasso-type estimators. *The Annals of statistics*, 28(5):1356–1378, 2000.
- Zijian Guo, Prabrisha Rakshit, Daniel S Herman, and Jinbo Chen. Inference for the case probability in high-dimensional logistic regression. *The Journal of Machine Learning Research*, 22(1):11480–11533, 2021.
- Jaroslav Hájek. Asymptotic normality of simple linear rank statistics under alternatives. *The Annals of Mathematical Statistics*, 39(2):325–346, 1968.
- Wassily Hoeffding. A class of statistics with asymptotically normal distribution. In *Breakthroughs in statistics*, pages 308–334. Springer, 1992.
- Kurt Hornik, Maxwell Stinchcombe, and Halbert White. Multilayer feedforward networks are universal approximators. *Neural networks*, 2(5):359–366, 1989.
- Steve Horvath. Dna methylation age of human tissues and cell types. *Genome biology*, 14(10):1–20, 2013.
- Svante Janson. The asymptotic distributions of incomplete u-statistics. *Zeitschrift für Wahrscheinlichkeitstheorie und Verwandte Gebiete*, 66(4):495–505, 1984.
- Adel Javanmard and Andrea Montanari. Confidence intervals and hypothesis testing for high-dimensional regression. *Journal of Machine Learning Research*, 15(1):2869–2909, 2014.
- Yuko Kato, David MJ Tax, and Marco Loog. A review of nonconformity measures for conformal prediction in regression. *Conformal and Probabilistic Prediction with Applications*, pages 369–383, 2023.
- Abbas Khosravi, Saeid Nahavandi, Doug Creighton, and Amir F Atiya. Lower upper bound estimation method for construction of neural network-based prediction intervals. *IEEE transactions on neural networks*, 22(3):337–346, 2010.
- Byol Kim, Chen Xu, and Rina Barber. Predictive inference is free with the jackknife+-after-bootstrap. *Advances in Neural Information Processing Systems*, 33:4138–4149, 2020.
- Michael Kohler and Adam Krzyżak. Adaptive regression estimation with multilayer feed-forward neural networks. *Nonparametric Statistics*, 17(8):891–913, 2005.

- Michael Kohler and Sophie Langer. On the rate of convergence of fully connected deep neural network regression estimates. *The Annals of Statistics*, 49(4):2231–2249, 2021.
- Shengchun Kong, Zhuqing Yu, Xianyang Zhang, and Guang Cheng. High dimensional robust inference for cox regression models using de-sparsified lasso. *Scandinavian Journal of Statistics*, 48(3):1068–1095, 2021. doi: 10.1111/sjos.12543.
- Kumarajarshi. Life expectancy (who), 2023. URL <https://www.kaggle.com/datasets/kumarajarshi/life-expectancy-who>. Kaggle dataset based on WHO data.
- A J Lee. *U-statistics: Theory and Practice*. Routledge, 2019.
- Jason D Lee, Dennis L Sun, Yuekai Sun, and Jonathan E Taylor. Exact post-selection inference, with application to the lasso. *The Annals of Statistics*, 44(3):907–927, 2016.
- Jing Lei, Max G’Sell, Alessandro Rinaldo, Ryan J Tibshirani, and Larry Wasserman. Distribution-free predictive inference for regression. *Journal of the American Statistical Association*, 113(523):1094–1111, 2018.
- Qiong Lin, Carola I Weidner, Ivan G Costa, Riccardo E Marioni, Marcelo RP Ferreira, Ian J Deary, and Wolfgang Wagner. Dna methylation levels at individual age-associated cpG sites can be indicative for life expectancy. *Aging (Albany NY)*, 8(2):394, 2016.
- Ake T Lu, Austin Quach, James G Wilson, Alex P Reiner, Abraham Aviv, Kenneth Raj, Lifang Hou, Andrea A Baccarelli, Yun Li, James D Stewart, et al. Dna methylation grimage strongly predicts lifespan and healthspan. *Aging (albany NY)*, 11(2):303, 2019.
- Riccardo E Marioni, Sonia Shah, Allan F McRae, Brian H Chen, Elena Colicino, Sarah E Harris, Jude Gibson, Anjali K Henders, Paul Redmond, Simon R Cox, et al. Dna methylation age of blood predicts all-cause mortality in later life. *Genome biology*, 16(1):1–12, 2015.
- Daniel F McCaffrey and A Ronald Gallant. Convergence rates for single hidden layer feedforward networks. *Neural Networks*, 7(1):147–158, 1994.
- Daniel L McCartney, Anna J Stevenson, Rosie M Walker, Jude Gibson, Stewart W Morris, Archie Campbell, Alison D Murray, Heather C Whalley, David J Porteous, Andrew M McIntosh, et al. Investigating the relationship between dna methylation age acceleration and risk factors for alzheimer’s disease. *Alzheimer’s & Dementia: Diagnosis, Assessment & Disease Monitoring*, 10:429–437, 2018.
- Lucas Mentch and Giles Hooker. Quantifying uncertainty in random forests via confidence intervals and hypothesis tests. *The Journal of Machine Learning Research*, 17(1):841–881, 2016.
- Soundouss Messoudi, Sébastien Destercke, and Sylvain Rousseau. Conformal multi-target regression using neural networks. In *Conformal and Probabilistic Prediction and Applications*, pages 65–83. PMLR, 2020.

- Lidija Milicic, Tenielle Porter, Michael Vacher, and Simon M Laws. Utility of dna methylation as a biomarker in aging and alzheimer’s disease. *Journal of Alzheimer’s Disease Reports*, 7(1):475–503, 2023.
- Yang Ning and Han Liu. A general theory of hypothesis tests and confidence regions for sparse high dimensional models. *The Annals of Statistics*, 45(1):158–195, 2017.
- Harris Papadopoulos. Inductive conformal prediction: Theory and application to neural networks. In *Tools in artificial intelligence*. Citeseer, 2008.
- Harris Papadopoulos, Volodya Vovk, and Alex Gammerman. Conformal prediction with neural networks. In *19th IEEE International Conference on Tools with Artificial Intelligence (ICTAI 2007)*, volume 2, pages 388–395. IEEE, 2007.
- Philippe Rigollet and Alexandre Tsybakov. Exponential screening and optimal rates of sparse estimation. *The Annals of Statistics*, 39(2):731–771, 2011.
- Yaniv Romano, Matteo Sesia, and Emmanuel Candes. Classification with valid and adaptive coverage. *Advances in Neural Information Processing Systems*, 33:3581–3591, 2020.
- Johannes Schmidt-Hieber. Nonparametric regression using deep neural networks with relu activation function. *The Annals of Statistics*, 48(4):1875–1897, 2020.
- Jordan Schupbach, John W Sheppard, and Tyler Forrester. Quantifying uncertainty in neural network ensembles using u-statistics. In *2020 International Joint Conference on Neural Networks (IJCNN)*, pages 1–8. IEEE, 2020.
- Karen Sugden, Avshalom Caspi, Maxwell L Elliott, Kyle J Bourassa, Kartik Chamarti, David L Corcoran, Ahmad R Hariri, Renate M Houts, Meeraj Kothari, Stephen Kritchevsky, et al. Association of pace of aging measured by blood-based dna methylation with age-related cognitive impairment and dementia. *Neurology*, 99(13):e1402–e1413, 2022.
- Ryan J Tibshirani, Rina Foygel Barber, Emmanuel Candes, and Aaditya Ramdas. Conformal prediction under covariate shift. In H. Wallach, H. Larochelle, A. Beygelzimer, F. d’ Alché-Buc, E. Fox, and R. Garnett, editors, *Advances in Neural Information Processing Systems*, volume 32. Curran Associates, Inc., 2019. URL https://proceedings.neurips.cc/paper_files/paper/2019/file/8fb21ee7a2207526da55a679f0332de2-Paper.pdf.
- Sara Van de Geer, Peter Bühlmann, Ya’acov Ritov, and Ruben Dezeure. On asymptotically optimal confidence regions and tests for high-dimensional models. *The Annals of Statistics*, 42(3):1166–1202, 2014.
- Aad W Van der Vaart. *Asymptotic Statistics*, volume 3. Cambridge University Press, 2000.
- Stefan Wager and Susan Athey. Estimation and inference of heterogeneous treatment effects using random forests. *Journal of the American Statistical Association*, 113(523):1228–1242, 2018.

- Martin J Wainwright. *High-dimensional statistics: A non-asymptotic viewpoint*, volume 48. Cambridge university press, 2019.
- Qing Wang and Yujie Wei. Quantifying uncertainty of subsampling-based ensemble methods under a u-statistic framework. *Journal of Statistical Computation and Simulation*, 92(17):3706–3726, 2022.
- Ming Yu, William D Hazelton, Georg E Luebeck, and William M Grady. Epigenetic aging: More than just a clock when it comes to cancer. *Cancer research*, 80(3):367–374, 2020.
- Jacob Zavatore-Veth, Abdulkadir Canatar, Ben Ruben, and Cengiz Pehlevan. Asymptotics of representation learning in finite bayesian neural networks. *Advances in neural information processing systems*, 34:24765–24777, 2021.
- Cun-Hui Zhang and Stephanie S Zhang. Confidence intervals for low dimensional parameters in high dimensional linear models. *Journal of the Royal Statistical Society: Series B (Statistical Methodology)*, 76(1):217–242, 2014.
- Yunyi Zhang and Dimitris N Politis. Bootstrap prediction intervals with asymptotic conditional validity and unconditional guarantees. *Information and Inference: A Journal of the IMA*, 12(1):157–209, 2023.
- Peng Zhao and Bin Yu. On model selection consistency of lasso. *Journal of Machine Learning Research*, 7(Nov):2541–2563, 2006.
- Yinchu Zhu and Jelena Bradic. Linear hypothesis testing in dense high-dimensional linear models. *Journal of the American Statistical Association*, 113(524):1583–1600, 2018.

Table 1: Simulation example 1: comparisons of prediction and inference for Lasso U-learning with various resample sizes, oracle prediction, and conformal prediction. *Note: We used true $f_0(\mathbf{x}_*)$ instead of y_* to derive conformal PIs for fair comparisons; SE is not available for conformal predictions.

	Bias	MAE	EmpSD	SE	CP	AIL
$n = 500, p = 3000$						
Oracle	0.003	0.009	0.088	0.093	0.956	0.366
$r = n^{0.8} = 144$	0.033	0.659	0.166	0.184	0.936	0.723
$r = n^{0.9} = 268$	0.013	0.328	0.119	0.137	0.952	0.538
$r = n^{0.95} = 366$	0.010	0.266	0.112	0.137	0.958	0.536
$r = n$ (SWR)	0.008	0.216	0.152	0.141	0.941	0.552
Naive Bootstrap	-0.003	0.213	0.283	0.240	0.781	0.941
Conformal PI*	0.018	0.349	0.211	-	0.961	1.884
$n = 1000, p = 3000$						
Oracle	-0.001	0.005	0.083	0.092	0.968	0.360
$r = n^{0.8} = 251$	0.016	0.539	0.143	0.143	0.969	0.562
$r = n^{0.9} = 501$	0.009	0.290	0.105	0.111	0.951	0.436
$r = n^{0.95} = 707$	0.007	0.236	0.101	0.112	0.947	0.441
$r = n$ (SWR)	0.005	0.170	0.160	0.146	0.965	0.571
Naive Bootstrap	0.008	0.172	0.283	0.235	0.78	0.923
Conformal PI	0.009	0.295	0.175	-	0.941	1.48

Table 2: Simulation example 2, DNN U-learning for prediction and inference. The last Time column is average computation time in seconds for one run.

	Bias	MAE	EmpSD	SE	CP	AIL	Time
Scenario 1							
$n = 200, r = n^{0.8}$	0.042	0.546	0.326	0.383	0.891	1.501	15
$r = n^{0.9}$	0.033	0.445	0.259	0.276	0.906	1.083	24
$r = n^{0.95}$	0.022	0.382	0.222	0.239	0.935	0.935	32
$n = 600, r = n^{0.8}$	0.048	0.314	0.174	0.204	0.983	0.8	105
$r = n^{0.9}$	0.030	0.230	0.170	0.195	0.954	0.803	109
$r = n^{0.95}$	0.022	0.189	0.168	0.184	0.942	0.840	135
Conformal PI	0.023	0.187	0.227	-	0.958	1.381	12
Scenario 2							
$n = 200, r = n^{0.8}$	0.082	0.737	0.199	0.211	0.887	0.825	22
$r = n^{0.9}$	0.080	0.520	0.215	0.221	0.937	0.866	24
$r = n^{0.95}$	0.080	0.476	0.216	0.238	0.945	0.934	27
$n = 600, r = n^{0.8}$	0.084	0.482	0.148	0.138	0.881	0.541	74
$r = n^{0.9}$	0.078	0.448	0.145	0.173	0.945	0.680	107
$r = n^{0.95}$	0.078	0.416	0.128	0.170	0.961	0.666	110
Conformal PI	0.093	0.430	0.214	-	0.969	2.335	13

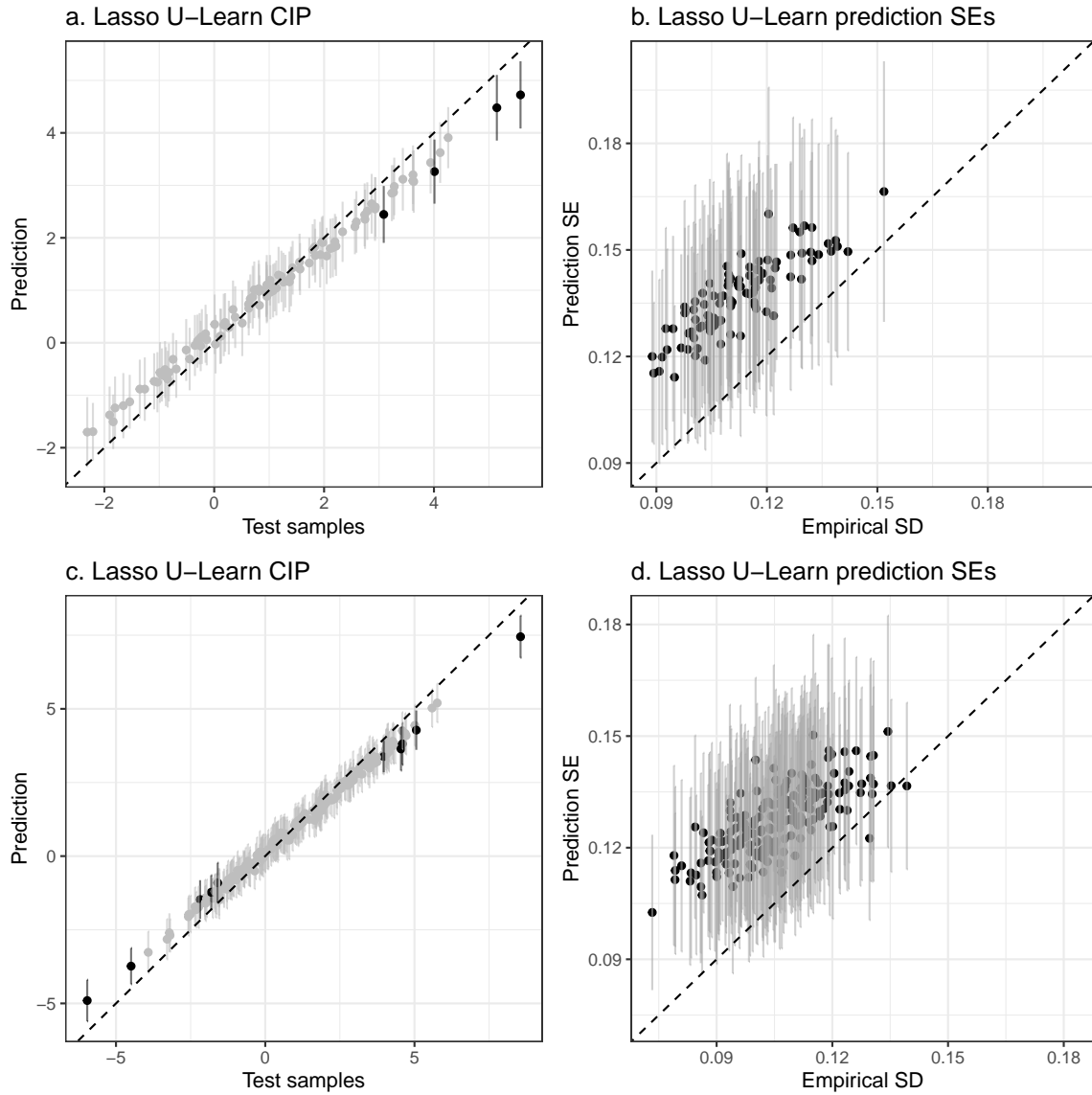


Figure 1: **Prediction and inference in simulation examples 1.** a,b) $n = 500$; c,d) $n = 1000$. Left panels show the average CIP on the test samples; right panels show the prediction SE versus the empirical SD of all test samples.

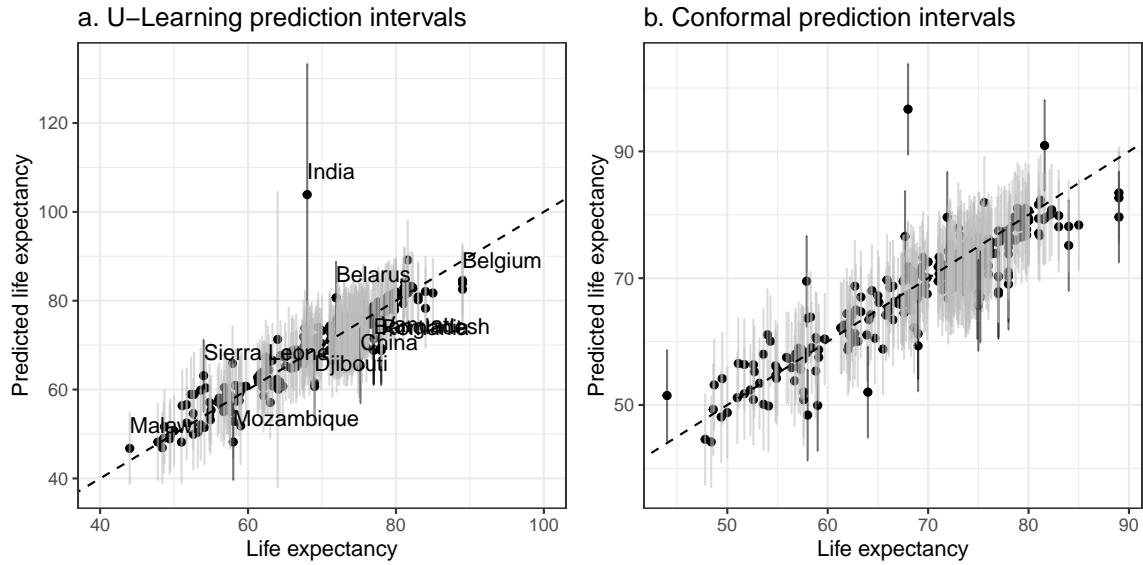


Figure 2: **Prediction intervals by U-learning (left) and Conformal Prediction (right) in Example 3 life expectancy data.** Prediction intervals that do not cover the truth are in black. The labeled countries in panel (a) are (from left to right): Malawi, Sierra Leone, Mozambique, India, Djibouti, Belarus, China, Bangladesh, Romania, Vanuatu, Belgium.

Table 3: DNAmAge prediction and inference in the human methylation data. Column names indicate the samples being evaluated and the model used in the parentheses.

	Blood (Lasso U-Learn)	Non-blood (Lasso U-Learn)	Test (Lasso U-Learn)	Test (DNN U-Learn)
Bias	-0.01	0.04	-0.45	-0.44
MAE	2.11	3.65	3.29	3.0
Corr	0.99	0.93	0.97	0.97
Mean SE	0.84	2.47	1.70	1.78
Min SE	0.24	1.22	0.42	0.65
Max SE	3.23	16.87	10.70	6.58
AIL	-	-	0.954	0.954

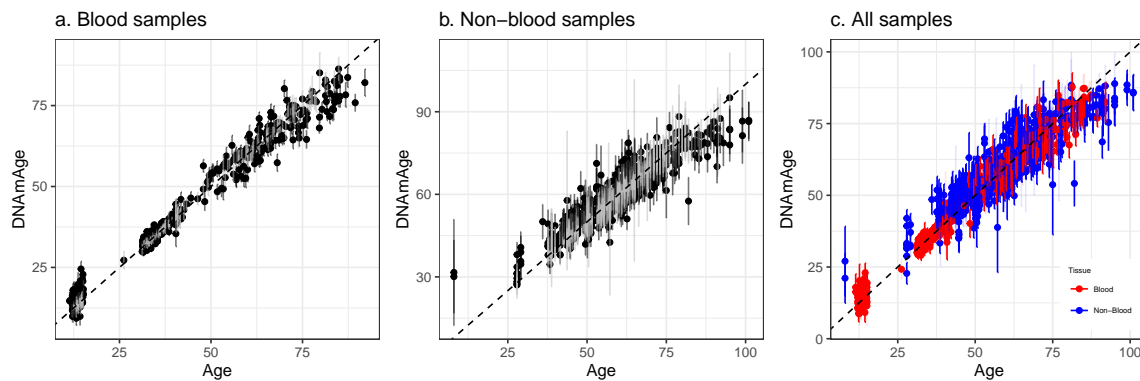


Figure 3: DNAmAge based on out-of-bag predictions and the prediction intervals in three clocks: a. blood samples; b. non-blood samples; c. all samples.

Table 4: Coverage of the U-learning PIs by health conditions on the test data. Fisher’s exact test is performed for each health condition versus the healthy individuals.

Cover	Total	Lasso U-Learn			DNN U-Learn		
		0	1	Fisher’s p	0	1	Fisher’s p
Healthy	72	0	72		0	72	
Alzheimer	11	4	7	< 0.001	4	7	< 0.001
ChronCond	50	3	47	0.07	1	49	0.41
HIV	140	5	135	0.17	7	133	0.10
OtherBrain	6	1	5	0.08	1	5	0.08
Parkinson	24	1	23	0.25	1	23	0.25

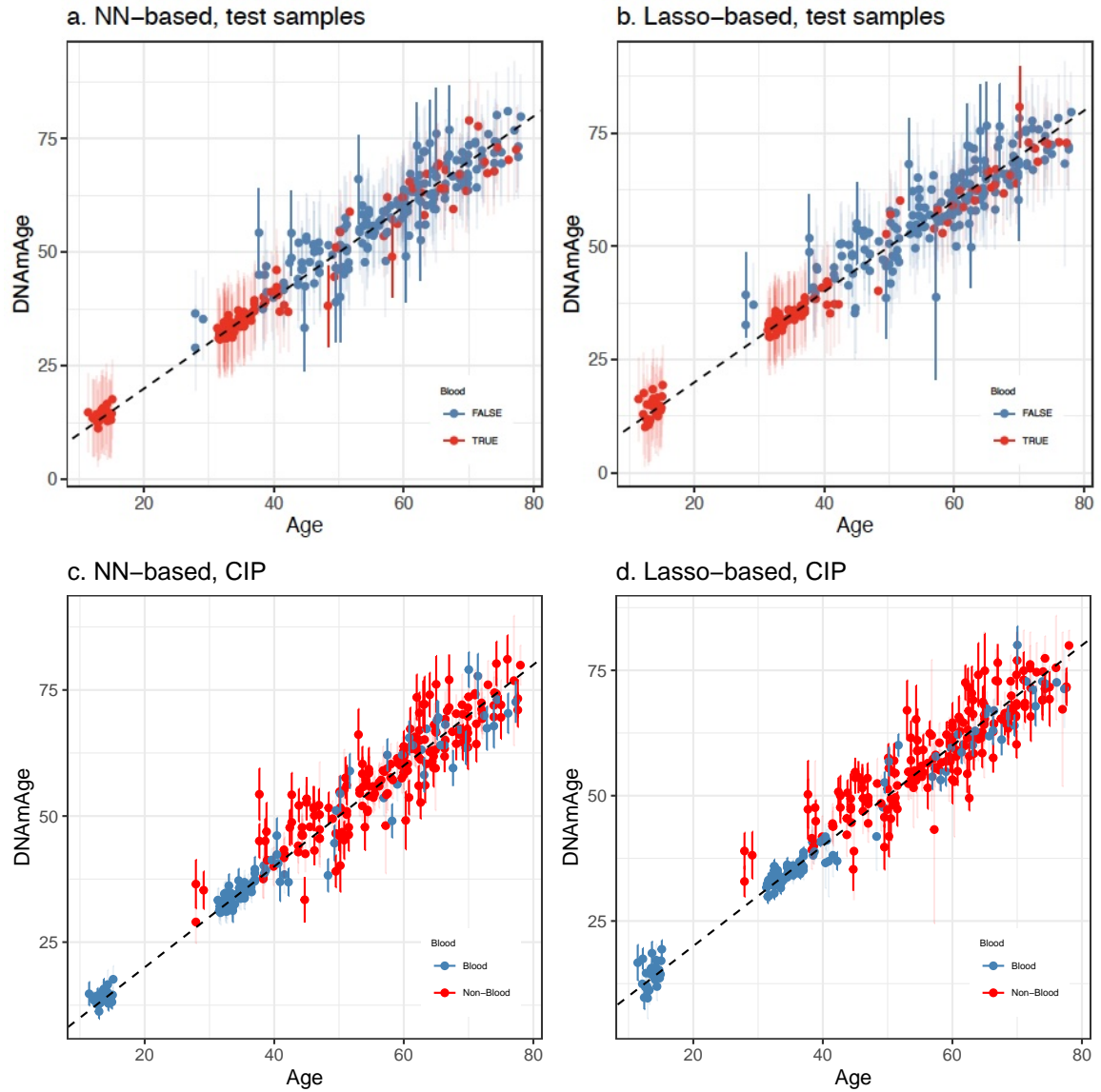


Figure 4: DNAmAge prediction intervals and CIP for all test samples based on two models.

Appendix: U-learning for Prediction Inference via Combinatory Multi-Subsampling: With Applications to LASSO and Neural Networks

Proofs of Theorem 2 and Corollary 3

We first introduce the following Lemma that gives a Lipschitz-type condition of the Lasso predictions on subsamples.

Lemma 7 *Consider the Lasso predictions based on subsamples $\mathcal{T}^1 = ((\mathbf{x}_1, y_1), \dots, (\mathbf{x}_r, y_r))$ and $\mathcal{T}^{1*} = ((\mathbf{x}_1, y_1), \dots, (\mathbf{x}_r, y_r^*))$, with $y_r = f_0(\mathbf{x}_r) + \varepsilon_r$, $y_r^* = f_0(\mathbf{x}_r) + \varepsilon_r^*$, ε_r and ε_r^* are i.i.d. errors satisfying (C1). There exists a constant c such that for all $r > 1$, the following Lipschitz-type condition is satisfied*

$$|\tilde{f}(\mathbf{x}_{r+1}; \mathcal{T}^1) - \tilde{f}(\mathbf{x}_{r+1}; \mathcal{T}^{1*})| \leq c|y_r - y_r^*|, \quad (10)$$

where \tilde{f} is defined in (4).

Proof Note that \mathcal{T}^1 and \mathcal{T}^{1*} only differ in the last observation, and for notational convenience, let $\varepsilon_i^* = \varepsilon_i$ for $i < r$. Within this proof, denote $\mathbf{X} = (\mathbf{x}_1^\top, \dots, \mathbf{x}_r^\top)^\top = (\mathbf{X}_1, \dots, \mathbf{X}_p)$, $\mathbf{Y} = (y_1, \dots, y_r)^\top$, and $\mathbf{y}_* = (y_1, \dots, y_r^*)^\top$. Define the set

$$C := \{\beta_1 \mathbf{X}_1 + \dots + \beta_p \mathbf{X}_p : \|\beta\|_1 \leq K\}$$

Further denote the Lasso solutions based on \mathcal{T}^1 and \mathcal{T}^{1*} as $\tilde{\beta}^K$ and $\tilde{\beta}^{*K}$ respectively. By definition, $\tilde{\mathbf{Y}} = \mathbf{X}\tilde{\beta}^K$ and $\tilde{\mathbf{Y}}^* = \mathbf{X}\tilde{\beta}^{*K}$ are the projections of \mathbf{Y} and \mathbf{y}_* onto C , respectively. Since C is convex, for any $\mathbf{v} \in C$, $(\mathbf{v} - \tilde{\mathbf{Y}}) \cdot (\mathbf{Y} - \tilde{\mathbf{Y}}) \leq 0$. Take $\mathbf{v} = \tilde{\mathbf{Y}}^*$, we have $(\tilde{\mathbf{Y}}^* - \tilde{\mathbf{Y}}) \cdot (\mathbf{Y} - \tilde{\mathbf{Y}}) \leq 0$. Then

$$\begin{aligned} \|\tilde{\mathbf{Y}}^* - \tilde{\mathbf{Y}}\|_2^2 &\leq (\mathbf{Y} - \tilde{\mathbf{Y}}^*) \cdot (\tilde{\mathbf{Y}} - \tilde{\mathbf{Y}}^*) \\ &= (\mathbf{Y} - \mathbf{y}_* + \mathbf{y}_* - \tilde{\mathbf{Y}}^*) \cdot (\tilde{\mathbf{Y}} - \tilde{\mathbf{Y}}^*) \\ &\leq (\mathbf{Y} - \mathbf{y}_*) \cdot (\tilde{\mathbf{Y}} - \tilde{\mathbf{Y}}^*) \\ &= (\varepsilon_r - \varepsilon_r^*) \mathbf{x}_r \cdot (\tilde{\beta}^K - \tilde{\beta}^{*K}). \end{aligned}$$

Note we used $(\mathbf{y}_* - \tilde{\mathbf{Y}}^*) \cdot (\tilde{\mathbf{Y}} - \tilde{\mathbf{Y}}^*) \leq 0$ and that \mathbf{Y} and \mathbf{y}_* only differed in the last observation in the above derivation. Denote $\tilde{\Delta} = \tilde{\beta}^K - \tilde{\beta}^{*K}$, and apply the Restricted Eigenvalue (RE) condition, we have

$$\begin{aligned} \kappa \|\tilde{\Delta}\|_2^2 &\leq \frac{1}{r} \|\tilde{\mathbf{Y}}^* - \tilde{\mathbf{Y}}\|_2^2 \\ &\leq |\varepsilon_r - \varepsilon_r^*| \frac{\|\mathbf{x}_r\|_\infty}{r} \|\tilde{\Delta}\|_1 \\ &\leq |\varepsilon_r - \varepsilon_r^*| \frac{\|\mathbf{x}_r\|_\infty}{r} 4\sqrt{s} \|\tilde{\Delta}\|_2. \end{aligned}$$

Note here $\tilde{\Delta}$ is the difference between the two Lasso solutions, hence s is not related to the sparsity of the true β^0 , rather depends on r and K with $s = o(r)$. Therefore,

$$\|\tilde{\Delta}\|_2 = \|\tilde{\beta}^K - \tilde{\beta}^{*K}\|_2 \leq \frac{4\sqrt{s}}{\kappa r} |\varepsilon_r - \varepsilon_r^*| \|\mathbf{x}_r\|_\infty,$$

where κ is the RE constant. Note it is a generalization of the classic ℓ_2 error bound on the Lasso solution (for example, Theorem 7.13(b) in Wainwright (2019)). Further denote $c_{r+1}^2 = \mathbf{x}_{r+1} \mathbf{x}_{r+1}^\top$, we have

$$\begin{aligned} \text{LHS of (10)} &= \left| \mathbf{x}_{r+1} \tilde{\boldsymbol{\beta}}^K - \mathbf{x}_{r+1} \tilde{\boldsymbol{\beta}}^{*K} \right| \\ &\leq \|\mathbf{x}_{r+1}\|_2 \|\tilde{\boldsymbol{\beta}}^K - \tilde{\boldsymbol{\beta}}^{*K}\|_2 \\ &\leq \frac{4c_{r+1} \sqrt{s}}{\kappa r} |\varepsilon_r - \varepsilon_r^*| \|\mathbf{x}_r\|_\infty \\ &\leq \frac{4c_{r+1} M \sqrt{s}}{\kappa r} |\varepsilon_r - \varepsilon_r^*|. \end{aligned}$$

Therefore, by choosing $c = \frac{4c_{r+1} M}{\kappa}$, (10) holds for all $r > 1$. \blacksquare

Before presenting the proof of Theorem 2, we introduce the Hájek projection (Van der Vaart, 2000; Wager and Athey, 2018), which helps the derivation of U-statistic properties. Given a complex statistic T and independent training samples Z_1, Z_2, \dots, Z_n , the Hájek projection of T is defined to be

$$\mathring{T} = \mathbb{E}[T] + \sum_{i=1}^n (\mathbb{E}[T|Z_i] - \mathbb{E}[T]),$$

i.e., a projection onto a linear subspace of all random variables of the form $\sum_{i=1}^n g_i(Z_i)$, where $g_i(\cdot)$ are measurable functions. It follows immediately that $\mathbb{E}(\mathring{T}) = \mathbb{E}(T)$.

As the Hájek projection \mathring{T} is a sum of independent random variables, we first show it is asymptotically normal under general conditions. Then, we set to bound the asymptotic difference between T and \mathring{T} , and by using Slutsky's theorem, show that the original T will be asymptotically normal as well.

Proof [Proof of Theorem 2] We present the proof in the following 3 key steps.

Step 1. Asymptotic normality of the Hájek projection. For notational ease, we first define

$$T_{n,r,B} = \hat{y}_*^B - f_0(\mathbf{x}_*),$$

and write its Hájek projection as

$$\mathring{T}_{n,r,B} = \sum_{i=1}^n \mathbb{E}(T_{n,r,B}|Z_i) = \sum_{i=1}^n \mathbb{E}(\hat{y}_*^B - f_0(\mathbf{x}_*)|Z_i), \quad (11)$$

where each term is

$$\begin{aligned} \mathbb{E}(\hat{y}_*^B - f_0(\mathbf{x}_*)|Z_i) &= \mathbb{E}\left(\frac{1}{B} \sum_{b=1}^B \tilde{f}^b(\mathbf{x}_*) - f_0(\mathbf{x}_*)|Z_i\right) \\ &= \frac{1}{B} \sum_{b=1}^B \mathbb{E}(\tilde{f}^b(\mathbf{x}_*) - f_0(\mathbf{x}_*)|Z_i). \end{aligned}$$

Let $h_{1,r}(x) = \mathbb{E}\tilde{f}^b(\mathbf{x}_*; x, Z_2, \dots, Z_r) - f_0(\mathbf{x}_*)$ and W be the number of subsamples that contain i , we have $W \sim \text{Binom}(B, \binom{n-1}{r-1}/\binom{n}{r})$, and it follows

$$\begin{aligned} \frac{1}{B} \sum_{b=1}^B \mathbb{E} \left(\tilde{f}^b(\mathbf{x}_*) - f_0(\mathbf{x}_*) | Z_i \right) &= \frac{1}{B} \sum_{b=1}^B \mathbb{E} \left(\mathbb{E}(\tilde{f}^b(\mathbf{x}_*) - f_0(\mathbf{x}_*) | Z_i) | W \right) \\ &= \frac{1}{B} \mathbb{E}(W h_{1,r}(Z_i)) \\ &= \frac{1}{B} \left(B \binom{n-1}{r-1} / \binom{n}{r} h_{1,r}(Z_i) \right) \\ &= \frac{r}{n} h_{1,r}(Z_i). \end{aligned}$$

Plug this back into (11) yields

$$\mathring{T}_{n,r,B} = \frac{r}{n} \sum_{i=1}^n h_{1,r}(Z_i).$$

To show the asymptotic normality of $\mathring{T}_{n,r,B}$, we can define the triangular array for $r_n h_{1,r_n}(Z_i)$'s and verify the Lindeberg condition as below. For any $\delta > 0$,

$$\begin{aligned} &\sum_{i=1}^n \frac{1}{nr_n^2 \xi_{1,r_n}} \int_{|r_n h_{1,r_n}(Z_i)| \geq \delta \sqrt{n \xi_{1,r_n}}} r_n^2 h_{1,r_n}^2(Z_i) dP \\ &= \sum_{i=1}^n \frac{1}{n \xi_{1,r_n}} \int_{|h_{1,r_n}(Z_i)| \geq \delta \sqrt{n \xi_{1,r_n}}} h_{1,r_n}^2(Z_i) dP \\ &= \frac{1}{\xi_{1,r_n}} \int_{|h_{1,r_n}(Z_1)| \geq \delta \sqrt{n \xi_{1,r_n}}} h_{1,r_n}^2(Z_1) dP. \end{aligned}$$

The above Lindeberg condition is satisfied by Lemma 7. To see it, we repeatedly apply (10) and Jensen's inequality to get the following bound,

$$\begin{aligned} &\sup_{\mathbf{x}_1 \in \mathcal{X}} |h_{1,r_n}((\mathbf{x}_1, y_1^*))| \\ &= \sup_{\mathbf{x}_1 \in \mathcal{X}} \left| \int \left(\tilde{f}((\mathbf{x}_1, y_1^*), (x_2, y_2), \dots, (x_{r_n}, y_{r_n})) - \tilde{f}((\mathbf{x}_1, y_1^*), \dots, (x_{r_n}, y_{r_n}^*)) \right) \right. \\ &\quad \left. + \tilde{f}((\mathbf{x}_1, y_1^*), \dots, (x_{r_n}, y_{r_n}^*)) dP - f_0 \right| \\ &\leq \sup_{\mathbf{x}_1 \in \mathcal{X}} \int \left(\tilde{f}((\mathbf{x}_1, y_1^*), (x_2, y_2), \dots, (x_{r_n}, y_{r_n})) - \tilde{f}((\mathbf{x}_1, y_1^*), \dots, (x_{r_n}, y_{r_n}^*)) \right) dP \\ &\quad + \sup_{\mathbf{x}_1 \in \mathcal{X}} \tilde{f}((\mathbf{x}_1, y_1^*), \dots, (x_{r_n}, y_{r_n}^*)) - f_0 \\ &\leq cr_n \mathbb{E} |\epsilon_1| + M - f_0. \end{aligned}$$

Then

$$\begin{aligned}
 A_n &= \left\{ |h_{1,r_n}((\mathbf{x}_1, y_1))| \geq \delta \sqrt{n\zeta_{1,r_n}} \right\} \\
 &= \left\{ |h_{1,r_n}((\mathbf{x}_1, y_1)) - h_{1,r_n}((\mathbf{x}_1, y_1^*)) + h_{1,r_n}((\mathbf{x}_1, y_1^*))| \geq \delta \sqrt{n\zeta_{1,r_n}} \right\} \\
 &\subseteq \left\{ |h_{1,r_n}((\mathbf{x}_1, y_1)) - h_{1,r_n}((\mathbf{x}_1, y_1^*))| \geq \delta \sqrt{n\zeta_{1,r_n}} - |h_{1,r_n}((\mathbf{x}_1, y_1^*))| \right\} \\
 &\subseteq \left\{ |\epsilon_1| \geq \frac{1}{c} \left(\delta \sqrt{n\zeta_{1,r_n}} + M - f_0 \right) + r_n \mathbb{E} |\epsilon_1| \right\} \\
 &:= A_n^*.
 \end{aligned}$$

In the above derivation, we used the bound

$$\sup_{\mathbf{x}_1 \in \mathcal{X}} |h_{1,r_n}((\mathbf{x}_1, y_1^*))| \leq cr_n \mathbb{E} |\epsilon_1| + M - f_0.$$

Further we have

$$\begin{aligned}
 &\frac{1}{\xi_{1,r_n}} \int_{A_n} h_{1,r_n}^2((\mathbf{x}_1, y_1)) dP \\
 &= \frac{1}{\xi_{1,r_n}} \int_{A_n} (h_{1,r_n}((\mathbf{x}_1, y_1)) - h_{1,r_n}((\mathbf{x}_1, y_1^*)) + h_{1,r_n}((\mathbf{x}_1, y_1^*)))^2 dP \\
 &\leq \frac{2}{\xi_{1,r_n}} \int_{A_n} (h_{1,r_n}((\mathbf{x}_1, y_1)) - h_{1,r_n}((\mathbf{x}_1, y_1^*)))^2 dP \\
 &\quad + \frac{2}{\xi_{1,r_n}} \int_{A_n} h_{1,r_n}^2((\mathbf{x}_1, y_1^*)) dP \\
 &\leq \frac{2}{\xi_{1,r_n}} \int_{A_n^*} c^2 \epsilon_1^2 dP + \frac{2}{\xi_{1,r_n}} P(A_n^*) (cr_n \mathbb{E} |\epsilon_1| + M - f_0)^2 \\
 &= \frac{2}{\xi_{1,r_n}} P \left[|\epsilon_1| \geq \frac{1}{c} (\sqrt{n\xi_{1,r_n}} + M - f_0) + \mathbb{E} |\epsilon_1| \right] \times (cr_n \mathbb{E} |\epsilon_1| + M - f_0)^2 \\
 &\rightarrow 0.
 \end{aligned}$$

Here the second inequality is by (10), and the last equality is due to the independence between A_n^* and ϵ_1 . Therefore the Lindeberg condition is satisfied, and by the Lindeberg-Feller central limit theorem,

$$\frac{\sqrt{n} \mathring{T}_{n,r,B}}{\sqrt{r_n^2 \xi_{1,r_n}}} \xrightarrow{d} N(0, 1). \tag{12}$$

Step 2. Asymptotic normality of $T_{n,r,B}$. The base learner $\tilde{T} = \tilde{f}(\mathbf{x}_*) - f_0(\mathbf{x}_*)$ is symmetric in the subsamples Z_1, Z_2, \dots, Z_r . The Efron-Stein ANOVA decomposition (Efron and Stein, 1981) states that there exist functions T_1, T_2, \dots, T_r such that

$$\tilde{T}(Z_1, Z_2, \dots, Z_r) = \sum_{i=1}^r T_1(Z_i) + \sum_{i < j} T_2(Z_i, Z_j) + \dots + T_r(Z_1, Z_2, \dots, Z_r),$$

and that all $2^r - 1$ random variables on the right hand side are all mean-zero and uncorrelated. Applying the ANOVA decomposition to each base learner in $T_{n,r,B}$ as in

$T_{n,r,B} = \widehat{y}_*^B - f_0(\mathbf{x}_*) = \frac{1}{B} \sum_{b=1}^B \widetilde{T}^b$ yields

$$T_{n,r,B} = \frac{1}{B} \left(\binom{n-1}{r-1} \sum_{i=1}^n T_1(Z_i) + \binom{n-2}{r-2} \sum_{i<j} T_2(Z_i, Z_j) + \dots + \sum_{i_1 < \dots < i_r} T_r(Z_{i_1}, \dots, Z_{i_r}) \right)$$

As with all projections,

$$\begin{aligned} \mathbb{E} \left[\left(T_{n,r,B} - \dot{T}_{n,r,B} \right)^2 \right] &= \text{Var} \left[T_{n,r,B} - \dot{T}_{n,r,B} \right] \\ &= \sum_{k=2}^r \left(\frac{r_k}{n_k} \right)^2 \binom{n}{k} V_k, \\ &= \sum_{k=2}^r \frac{r_k}{n_k} \binom{r}{k} V_k, \\ &\leq \frac{r_2}{n_2} \sum_{k=2}^r \binom{r}{k} V_k, \\ &\leq \frac{r_2}{n_2} \text{Var} [\widetilde{T}], \end{aligned}$$

where $V_k = \text{Var}(T_k)$ and $r_k = r(r-1)\dots(r-k)$. Lastly, $r_2/n_2 \leq r^2/n^2$.

Write $\text{Var}(\dot{T}_{n,r,B}) = v_n^2/n = r_n^2 \xi_{1,r_n}/n$, we have

$$\frac{1}{\text{Var}(\dot{T}_{n,r,B})} \mathbb{E} \left[\left(T_{n,r,B} - \dot{T}_{n,r,B} \right)^2 \right] \leq \left(\frac{r}{n} \right)^2 \frac{\text{Var}[\widetilde{T}]}{r_n^2 \xi_{1,r_n}/n} \quad (13)$$

$$= \frac{1}{n} \text{Var}[\widetilde{T}] / \xi_{1,r_n} \quad (14)$$

$$\rightarrow 0. \quad (15)$$

Apply Slutsky's theorem to (12) and (15), we get

$$\frac{\sqrt{n} T_{n,r,B}}{\sqrt{r_n^2 \xi_{1,r_n}}} \xrightarrow{d} N(0, 1).$$

Step 3. Consistency of the variance estimator. We are only left to show $n \widehat{V}^B / v_n^2 \xrightarrow{p} 1$, or equivalently $\widehat{V}^B / \text{Var}(\dot{T}_{n,r,B}) \xrightarrow{p} 1$.

From its definition, $\text{Var}(\dot{T}_{n,r,B})$ can be written as

$$\begin{aligned} \delta_n^2 &= \sum_{i=1}^n \left(\mathbb{E}[\widehat{y}_*^B | Z_i] - \mathbb{E}[\widehat{y}_*^B] \right)^2 \\ &= \frac{r^2}{n^2} \sum_{i=1}^n \left(\mathbb{E}[\widetilde{y}_*^b | Z_i] - \mathbb{E}[\widetilde{y}_*^b] \right)^2. \end{aligned} \quad (16)$$

This is because $E[\tilde{y}_*^b|Z_i] - E[\tilde{y}_*^b] = 0$ for those subsamples where Z_i is not sampled. On the other hand, we write the infinitesimal jackknife estimate as

$$\widehat{V}^B = \frac{n-1}{n} \left(\frac{n}{n-r} \right)^2 \frac{r^2}{n^2} \sum_{i=1}^n \left(E^*[\tilde{y}_*^b|Z_1^* = Z_i] - E^*[\tilde{y}_*^b] \right)^2. \quad (17)$$

It is worth noting that that E is with respect to the true (theoretical) distribution that generates Z_1, Z_2, \dots, Z_n , whereas E^* is with respect to the empirical distribution based on Z_1, Z_2, \dots, Z_n .

Equation (17) can further be decomposed using the Hájek projection \dot{y}^* of \tilde{y}_*^b :

$$\widehat{V}^B = \frac{n-1}{n} \left(\frac{n}{n-r} \right)^2 \frac{r^2}{n^2} \sum_{i=1}^n (A_i + R_i)^2, \quad (18)$$

where

$$\begin{aligned} A_i &= E^*[\dot{y}^*|Z_1^* = Z_i] - E^*[\dot{y}^*], \\ R_i &= E^*[\tilde{y}_*^b - \dot{y}^*|Z_1^* = Z_i] - E^*[\tilde{y}_*^b - \dot{y}^*]. \end{aligned}$$

We will show the main effects A_i 's give us δ_n^2 and the sum of R_i 's goes to zero. Therefore, $\lim_{n \rightarrow \infty} \widehat{V}^B / \text{Var}[T_{n,r,B}^{\circ}] = 1$. To show it, we write

$$\begin{aligned} A_i &= E^*[\dot{y}^*|Z_1^* = Z_i] - E^*[\dot{y}^*] \\ &= \left(1 - \frac{r}{n}\right) T_1(Z_i) + \left(\frac{r-1}{n-1} - \frac{r}{n}\right) \sum_{j \neq i} T_1(Z_j), \end{aligned}$$

where $T_1(Z_i) = E[\tilde{y}_*^b|Z_i] - E[\tilde{y}_*^b]$, and further

$$\begin{aligned} E \left[\frac{n-1}{n} \left(\frac{n}{n-r} \right)^2 \frac{r^2}{n^2} \sum_{i=1}^n A_i^2 \right] &= \frac{r^2}{n^2} \sum_{i=1}^n T_1(Z_i)^2 \\ &= \delta_n^2. \end{aligned}$$

From the above calculation we can also get $\delta_n^{-2} \frac{r^2}{n^2} \sum_{i=1}^n (A_i - T_1(Z_i))^2 \rightarrow_p 0$. Thus by the weak law of large numbers for triangular arrays for $\frac{1}{\delta_n^2} \frac{r^2}{n^2} \sum_{i=1}^n T_1(Z_i)^2$, we have

$$\frac{1}{\delta_n^2} \frac{r^2}{n^2} \sum_{i=1}^n A_i^2 \rightarrow_p 1.$$

On the other hand, we can get the following bound following Lemma 13 of Wager and Athey (2018),

$$E[R_i^2] \lesssim \frac{2}{n} \text{Var}[\tilde{y}_*^b],$$

which leads to

$$\begin{aligned} E \left[\frac{r^2}{n^2} \sum R_i^2 \right] &\lesssim \frac{2r^2}{n^2} \text{Var}[\tilde{y}_*^b] \\ &\lesssim \frac{2r}{n} \delta_n^2. \end{aligned}$$

The last step used the decomposition (16) and $\delta_n^2 = \frac{r}{n} \text{Var} [\tilde{y}_*^b]$. Then by Markov's inequality, as $r/n \rightarrow 0$,

$$\frac{1}{\delta_n^2} \frac{r^2}{n^2} \sum R_i^2 \xrightarrow{p} 0.$$

Lastly, applying $(A_i + R_i)^2 \leq 2(A_i^2 + R_i^2)$ to (18), we conclude that \widehat{V}^B/δ_n^2 converges in probability to 1. ■

Proof [Proof of Corollary 3] With the results of Step 3 in the proof of Theorem 2 and by using the Slutsky theorem, we have that

$$\frac{\widehat{y}_*^B - f_0(\mathbf{x}_*)}{\widehat{\sigma}_*} \xrightarrow{d} N(0, 1).$$

Therefore,

$$\begin{aligned} \Pr \left[f_0(\mathbf{x}_*) \in \left(\widehat{L}(\mathbf{x}_*), \widehat{U}(\mathbf{x}_*) \right) \right] &= \Pr \left[\left| \frac{f_0(\mathbf{x}_*) - \widehat{y}_*^B}{\widehat{\sigma}_*} \right| < z_{1-\alpha/2} \right] \\ &\rightarrow \Pr[|N(0, 1)| < z_{1-\alpha/2}] = 1 - \alpha. \end{aligned}$$
■

DNN U-learning

The proof of Theorem 5 uses arguments for incomplete generalized U-statistics with random kernels, i.e., each $\tilde{f}^{b_j}(\mathbf{x})$ is not deterministic given the subsample of training data. The key is that the randomness in $\tilde{f}^{b_j}(\mathbf{x})$ is independent of the original samples. Our proof takes advantage of the U-statistic property that the asymptotic normality does not depend on the exact form of the kernel, which is the NN fit in this case.

Proof [Proof of Theorem 5] Denote ω_j as the randomization parameters (SGD, random dropout, etc) involved in fitting the NN with the j -th subsample in Algorithm 2.

$$\begin{aligned} \tilde{f}^{b_j}(\mathbf{x}) &= \tilde{f}^{(\omega_j)}(\mathbf{x}|L, \mathbf{p}, \mathcal{T}^{b_j}) \\ \widehat{y}_*^B &= \frac{1}{B} \sum_j \tilde{f}^{b_j}(\mathbf{x}_*) = \frac{1}{B} \sum_j \tilde{f}^{(\omega_j)}(\mathbf{x}_*|L, \mathbf{p}, \mathcal{T}^{b_j}). \end{aligned}$$

Suppose $\omega_1, \dots, \omega_B \sim_{i.i.d.} F_\omega$, and they are independent of the observations \mathcal{T}_n and the random subsampling. Consider the statistic $\widehat{y}_*^{*B} = \mathbb{E}_\omega \widehat{y}_*^B$ by taking the expectation with respect to ω . Then \widehat{y}_*^{*B} is an incomplete generalized U-statistic by definition.

In order to apply Theorem 2 to \widehat{y}_*^{*B} , we verify the required conditions as follows. First, (D1) is analogous to (C1), (D2) and (C2) are identical, (D3) and (D4) together bound the tail behavior of the error term and the predictions $\tilde{f}^{b_j}(\mathbf{x}_*)$'s. By Lemma 4,

$$R(\tilde{f}^{b_j}, f_0) \leq C' \phi_n L \log^2 r_n.$$

Equivalently,

$$\mathbb{E} \left[\left(\tilde{f}^{b_j}(\mathbf{x}_*) - f_0(\mathbf{x}_*) \right)^2 \right] \leq C' \phi_n L \log^2 r_n.$$

Then

$$\begin{aligned} \mathbb{E} \left(\hat{y}_*^{*B} - f_0(\mathbf{x}_*) \right)^2 &= \mathbb{E} \left(\mathbb{E}_\omega \hat{y}_*^B - f_0(\mathbf{x}_*) \right)^2 \\ &= \mathbb{E} \left[\mathbb{E}_\omega \left(\hat{y}_*^B - f_0(\mathbf{x}_*) \right)^2 \right] \\ &= \mathbb{E} \left[\mathbb{E}_\omega \left(\frac{1}{B} \sum_{j=1}^B \tilde{f}^{b_j}(\mathbf{x}_*) - f_0(\mathbf{x}_*) \right)^2 \right] \\ &\leq \mathbb{E} \left[\mathbb{E}_\omega \frac{1}{B} \sum_{j=1}^B \left(\tilde{f}^{b_j}(\mathbf{x}_*) - f_0(\mathbf{x}_*) \right)^2 \right] \\ &\leq C' \phi_n L \log^2 r_n \\ &\lesssim \phi_n (\log^\alpha n) (\log^2 r_n) \\ &\lesssim \phi_n \log^{2+\alpha} n, \end{aligned}$$

which goes to zero by Lemma 4. Here, the last inequality is because of (D2).

Therefore, $\mathbb{E} \hat{y}_*^{*B} \rightarrow f_0(\mathbf{x}_*)$. Let

$$\xi_{1,r_n}(\mathbf{x}_*) = \text{Cov} \left(\tilde{f}^{(\omega)}(\mathbf{x}_*; Z_1, Z_2, \dots, Z_{r_n}), \tilde{f}^{(\omega)}(\mathbf{x}_*; Z_1, Z_2', \dots, Z_{r_n}') \right),$$

where the covariance is taken over ω as well. Since $\tilde{f}^{(\omega)} \in \mathcal{F}(L, \mathbf{p}, s, F)$ with a uniform upper bound F , $\mathbb{E} \{ \tilde{f}^{(\omega)}(\mathbf{x}) \}^2 \leq F^2 < \infty$. Hence, the non-random version $\hat{y}_*^{*B} = \mathbb{E}_\omega \hat{y}_*^B$ satisfies all the conditions of Theorem 2, and we can obtain

$$\frac{\sqrt{n} \left(\hat{y}_*^{*B} - f_0(\mathbf{x}_*) \right)}{v_n(\mathbf{x}_*)} \xrightarrow{d} N(0, 1),$$

with $v_n(\mathbf{x}_*) = \sqrt{r_n^2 \xi_{1,r_n}(\mathbf{x}_*)}$. Therefore, in order to show the asymptotic normality for \hat{y}_*^B , we are left to show

$$\frac{\sqrt{n} \left(\hat{y}_*^{*B} - \hat{y}_*^B \right)}{v_n(\mathbf{x}_*)} \xrightarrow{P} 0. \quad (19)$$

To proceed, we first write out the following expression, and derive

$$\begin{aligned} \mathbb{E} \left(\hat{y}_*^B - \hat{y}_*^{*B} \right)^2 &= \mathbb{E} \left[\frac{1}{B} \sum_j \tilde{f}^{(\omega_j)}(\mathbf{x}_* | \mathcal{T}^{b_j}) - \mathbb{E}_\omega \left(\frac{1}{B} \sum_j \tilde{f}^{(\omega_j)}(\mathbf{x}_* | \mathcal{T}^{b_j}) \right) \right]^2 \\ &= \mathbb{E} \left[\frac{1}{B^2} \sum_j \left(\tilde{f}^{(\omega_j)}(\mathbf{x}_* | \mathcal{T}^{b_j}) - \mathbb{E}_\omega \tilde{f}^{(\omega_j)}(\mathbf{x}_* | \mathcal{T}^{b_j}) \right)^2 \right] \\ &= \frac{1}{B^2} \sum_j \mathbb{E} \left(\tilde{f}^{(\omega_j)}(\mathbf{x}_* | \mathcal{T}^{b_j}) - \mathbb{E}_\omega \tilde{f}^{(\omega_j)}(\mathbf{x}_* | \mathcal{T}^{b_j}) \right)^2 \\ &= \frac{1}{B} \mathbb{E} \left(\tilde{f}^{(\omega_j)}(\mathbf{x}_* | \mathcal{T}^{b_j}) - \mathbb{E}_\omega \tilde{f}^{(\omega_j)}(\mathbf{x}_* | \mathcal{T}^{b_j}) \right)^2. \end{aligned}$$

Then for any $\epsilon_0 > 0$, applying the Chebyshev inequality gives

$$\Pr \left(\left| \frac{\sqrt{n} (\hat{y}_*^{*B} - \hat{y}_*^B)}{v_n(\mathbf{x}_*)} \right| > \epsilon_0 \right) \leq \frac{1}{\epsilon_0^2 v_n^2(\mathbf{x}_*)} \mathbb{E} \{ n (\hat{y}_*^{*B} - \hat{y}_*^B)^2 \}.$$

On the other hand, we have

$$\begin{aligned} & \frac{1}{\epsilon_0^2 v_n^2(\mathbf{x}_*)} \mathbb{E} \{ n (\hat{y}_*^{*B} - \hat{y}_*^B)^2 \} \\ &= \frac{1}{\epsilon_0^2} \frac{1}{r_n^2 \xi_{1,r_n}(\mathbf{x}_*)} \frac{n}{B} \mathbb{E} \left(\tilde{f}^{(\omega_j)}(\mathbf{x}_* | \mathcal{T}^{b_j}) - \mathbb{E}_\omega \tilde{f}^{(\omega_j)}(\mathbf{x}_* | \mathcal{T}^{b_j}) \right)^2 \\ & \rightarrow 0, \end{aligned}$$

which holds because, by assumptions, $n/B \rightarrow 0$, $\liminf \xi_{1,r_n}(\mathbf{x}_*) > 0$, and

$$\lim_{n \rightarrow \infty} \mathbb{E} \left(\tilde{f}^{(\omega_j)}(\mathbf{x}_* | \mathcal{T}^{b_j}) - \mathbb{E}_\omega \tilde{f}^{(\omega_j)}(\mathbf{x}_* | \mathcal{T}^{b_j}) \right)^2 < \infty.$$

Therefore, $\Pr \left(\left| \frac{\sqrt{n} (\hat{y}_*^{*B} - \hat{y}_*^B)}{v_n(\mathbf{x}_*)} \right| > \epsilon_0 \right) \rightarrow 0$ for any $\epsilon_0 > 0$. Hence (19) holds, and the proof is completed by applying the Slutsky theorem. ■